Study of the (d, p) Reaction on the Even-A Barium Isotopes 130–138†

D. von Ehrenstein,* G. C. Morrison, J. A. Nolen, Jr.,‡ and N. Williams§
Argonne National Laboratory, Argonne, Illinois 60439

(Received 22 December 1969)

The (d,p) reactions on $Ba^{130,132,134,136,138}$ have been investigated with 12.0-MeV deuterons from the Argonne Tandem Van de Graaff accelerator. Proton spectra were recorded in a broad-range magnetic spectrograph. Many new levels were observed. The ground-state Q values (in MeV) for the (d,p) reactions (including the odd-A targets) are found to be 5.269 for $A=130$, 4.977 for $A=132$, 4.746 for $A=134$, 6.886 for $A=135$, 4.680 for $A=136$, 6.398 for $A=137$, and 2.493 for $A=138$. Proton angular distributions were measured for states up to an excitation energy of about 3 MeV. The observed angular momentum transfers were $l_n = 0$, 1, 2, 3, and 5, which correspond to the population of states of the $3s_{1/2}$ and $2d_{3/2}$ configurations below the closed neutron shell at $N=82$ and the $2f_{7/2}$, $3p_{3/2}$, $3p_{1/2}$, $1h_{9/2}$, and $2f_{5/2}$ configurations above it. From the observed l values, it was possible to assign spins in some isotopes from a knowledge of the spin in other isotopes by taking account of systematic shifts in the Q values of levels and also from shell-model expectations. Distorted-wave Born-approximation calculations were used to extract absolute spectroscopic factors. The problems and uncertainties arising in such calculations were studied in some detail. They derive, in part, from the need to use a sharp radial cutoff to fit the experimental angular distributions; calculations with nonlocal potentials and finite-range approximations did not yield satisfactory fits. Another source of uncertainty is the dependence of the spectroscopic factors upon the geometric parameters of the bound-state potential well. The results are interpreted with the help of pairing theory; centers of gravity and single-particle energies are deduced.

I. INTRODUCTION

Investigation of the nuclear structure of the barium isotopes is of interest because this element has many stable isotopes, which span the range of neutron numbers from $N=74$ (Ba^{130}) to the closed $N=82$ shell (Ba^{138}). Thus a study of the (d,p) reaction on these isotopes can locate the position of the various single-particle levels above and below $N=82$ and the order in which the orbits are depleted as one departs from the closed $N=82$ shell.

Previous investigations of $N=82$ isotopes include several on the $Ba^{138}(d,p)Ba^{139}$ reaction[1-5] and (d,p) reactions on other $N=82$ targets with different proton number Z.[3,4,6-8] Such studies have identified single-particle levels above $N=82$ and have established that the neutron levels in the $N=83$ nuclei are relatively independent of proton number. Less work has been performed on targets with proton number in the same range but $N\neq 82$. In the case of the even-A Ba target isotopes, the only results are from a low-resolution study of the $Ba^{136}(d,p)Ba^{137}$ reaction.[1] The (d,p) reactions on the even-A targets, Ba^{134} to Ba^{130}, have not been reported previously.

The present work is part of an extensive study of the barium nuclei by means of the (d,p) reaction, the (d,d) reaction, and elastic and inelastic proton scattering at isobaric analog resonances – all with the stable Ba isotopes as targets.[9-14] Only the results for the (d,p) reaction on the even-A isotopes are reported here; subsequent publications will be concerned with the results obtained for the other reactions.

The study was motivated initially by the observation[9,15] of analog resonances in elastic proton scattering on the Ba isotopes. In order to correlate the observed analog resonances with the parent states in the odd-A Ba isotopes, the (d,p) reactions on the even-mass isotopes were investigated. Thus a main goal of this work is the determination of reliable spectroscopic factors for comparison with the equivalent spectroscopic factors obtained from analysis of the corresponding analog resonances in proton elastic scattering from the same target.[16]

Compared with most previous (d,p) studies in this mass region, the present work measures angular distributions to more forward angles. Considerable effort was also expended on establishing accurate values of the absolute cross sections. In addition, a rather comprehensive study of the distorted-wave Born-approximation (DWBA) procedure has been carried out. It was found that the most severe uncertainty in the calculation of absolute spectroscopic factors stems from the large sensitivity to small changes in the radius and diffuseness of the potential of the bound state into which the neutron is captured. To test this sensi-

tivity, we have extended the analysis of Sharpey-Schafer, who had pointed out that the rms radius of the bound-state potential well may be the important parameter in determining spectroscopic factors.[17] This observation was prompted by the reformulated optical model of Greenlees, Pyle, and Tang.[18] Further uncertainties arise from difficulties in fitting the shapes of the experimental angular distributions with DWBA calculations. The use of zero-range local potentials (with and without sharp radial cutoff) as well as finite-range nonlocal potentials in the analysis is examined.

In spite of these difficulties, the experimental angular distributions appear uniquely characteristic of a particular l value, and hence the l value extraction was unambiguous. We observed transitions to the $2d_{3/2}$ and $3s_{1/2}$ orbits below the $N=82$ neutron shell and to the $2f_{7/2}$, $3p_{3/2}$, $3p_{1/2}$, $1h_{9/2}$, and $2f_{5/2}$ orbits above it. Only secondary attention was given to weakly excited levels, and measurements were not extended to high enough excitation energies to guarantee that components of these single-particle levels were observed.

II. EXPERIMENTAL PROCEDURE

Angular distributions and absolute cross sections for the (d,p) reactions on the Ba targets were measured with 12.0-MeV deuterons accelerated by the Argonne Tandem Van de Graaff. Measurements were performed at angles between 5 and 50° with the broad-range magnetic spectrograph[19]; in some cases measurements were extended to 80°. The observed resolution width was typically about 13–15 keV (full width at half maximum).

The target material was obtained from Oak Ridge National Laboratory as barium nitrate. Table I gives the isotopic composition for each of the separated barium targets. Unfortunately it was not possible to identify the peaks of contaminant barium isotopes by means of the kinematics of the reactions.

Targets about 250 μg/cm^2 thick were prepared by evaporating metallic Ba onto a carbon backing about 20 μg/cm^2 thick. The barium nitrate was heated in a tantalum tube to about 400°C to form barium oxide, which was then reduced by the surface of the tantalum tube at about 2000°C to release the barium metal. The targets were prepared, transferred into the scattering chamber, and stored *in vacuo* by means of a vacuum lock system. Freshly prepared targets could be exposed to 400–600 nA of deuterons at 12 MeV without fracture, but the limit for older targets was only 200–300 nA. The energy loss was about 8 keV for the 12-MeV incident deuterons and about 4 keV for the outgoing protons in the present experiment.

TABLE I. Percentage composition of the enriched barium targets (precision about 0.1%).

	Isotopic abundances (%)						
Target	Ba^{130}	Ba^{132}	Ba^{134}	Ba^{135}	Ba^{136}	Ba^{137}	Ba^{138}
Ba^{130}	48.3	0.21	2.34	4.86	4.7	5.72	33.9
Ba^{132}	<0.1	39.2	4.55	7.74	6.2	6.58	35.7
Ba^{134}	<0.02	<0.02	85.9	3.65	1.79	1.59	7.11
Ba^{136}	<0.05	<0.05	0.07	0.81	92.9	1.75	4.54
Ba^{138}	<0.01	<0.01	<0.01	<0.02	<0.02	0.20	99.8

The protons were detected in Kodak NTB plates 50 μ thick, covered with 15-mil acetate foil in order to eliminate deuteron tracks and to intensify proton tracks. By use of zone masks, either of two solid angles of the magnetic spectrograph can be selected: about 3×10^{-4} sr or about 10^{-3} sr. The larger solid angle was used in half of the exposures. The total charge incident on the target was measured in a current integrator and ranged from 250 to 2000 μC. The exposures were monitored with a surface-barrier detector.

A major effort was made to obtain accurate absolute cross sections. These measurements for all targets were performed with the spectrograph; and for Ba^{138} and Ba^{136} targets they were repeated with solid-state detectors in an 18-in. scattering chamber.[20] The target thickness was determined by counting the elastically scattered deuterons at 25° for incident energies of 4 and 6 MeV. An optical-model calculation using the program ABACUS[21] with several sets of parameters showed that the deviation from Rutherford scattering is at most 1 part in 10^4 under these circumstances. An additional measurement was made (in the spectrograph only) with 12-MeV deuterons at $\theta_{lab}=13°$; for this the calculation showed a 1–2% deviation from Rutherford scattering. The measurement in the 18-in. scattering chamber included a careful check of the detector angle and of the position of the target. This was accomplished (1) by checking that the detector motion was centered accurately on the target, (2) by verifying the left-right symmetry, and (3) by measuring the Rutherford scattering of 6-MeV deuterons from Ba^{138} between 30 and 70°; the experimental deviation from the Rutherford cross section was found to be within ±1%. The results at 4, 6, and 12 MeV were in agreement within the errors (total error ≈ ±2.5%). Long (d,p) exposures were then taken under identical conditions, and the absolute cross sections were calculated.

The absolute Q value of the $Ba^{138}(d,p)$ reaction to the ground state was determined at backward

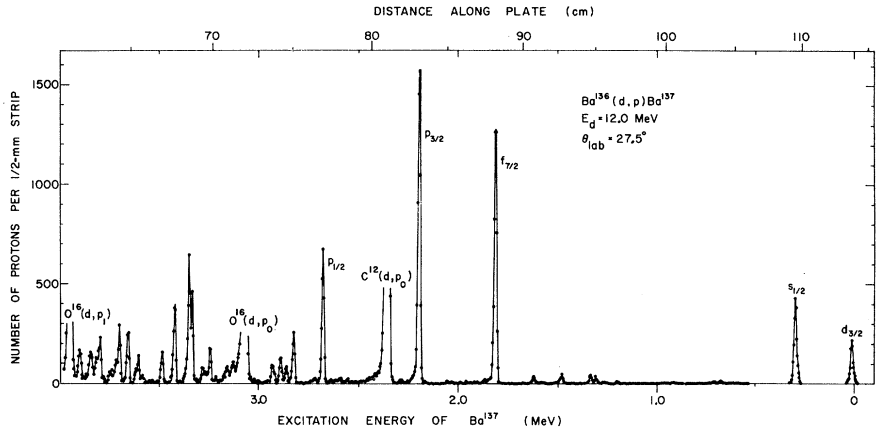

FIG. 1. Proton spectrum from the $Ba^{136}(d,p)Ba^{137}$ reaction. The strongest peaks are labeled with their single-particle configuration.

angles, with the target in reflection and with no absorbing foil in front of the emulsion. This was in agreement with the Q value obtained in the forward direction after correcting for the target thickness and for the displacement of the emulsions by the 15-mil acetate foil. The Q values of the other targets were determined in forward directions. In addition, the contaminant peaks due to Ba^{138} impurities in these barium isotopes (Table I) were used to obtain relative Q values. The determination of the absolute Q values relied upon the energy calibration of the magnetic spectrograph[22] and included several measurements of the precise tandem energy by elastic scattering of the incident deuteron beam.

III. RESULTS

A typical spectrum measured in the broad-range magnetic spectrograph is shown in Fig. 1. In this spectrum from the $Ba^{136}(d,p)Ba^{137}$ reaction, peaks corresponding to the ground state, the first excited state, and a few states at medium excitation energy in Ba^{137} stand out very clearly and are labeled with their orbital and their total angular momenta.

TABLE II. Measured Q values (MeV) of the $Ba(d,p)$ ground-state reactions.

Reaction	This work	Mass table[a]
$Ba^{130}(d,p)Ba^{131}$	5.269 ± 0.015	5.408 ± 0.027
$Ba^{132}(d,p)Ba^{133}$	4.977 ± 0.015	5.139 ± 0.282
$Ba^{134}(d,p)Ba^{135}$	4.746 ± 0.015	4.975 ± 0.107
$Ba^{135}(d,p)Ba^{136}$	6.886 ± 0.015	7.007 ± 0.128
$Ba^{136}(d,p)Ba^{137}$	4.680 ± 0.015	4.727 ± 0.106
$Ba^{137}(d,p)Ba^{138}$	6.398 ± 0.015	6.317 ± 0.086
$Ba^{138}(d,p)Ba^{139}$	2.493 ± 0.010[b,c]	2.487 ± 0.071

[a] See Ref. 23.

[b] Reported as 2.493 ± 0.010 MeV by C. H. Paris, W. W. Buechner, and P. M. Endt, Phys. Rev. 100, 1317 (1955).

[c] Reference 4 obtains 2.496 ± 0.015 MeV.

The absolute Q values for the ground-state transitions are given in Table II, where they are compared with previous values given in the mass tables.[23] The Q_0 values for the (d,p) reaction on the two odd-mass targets Ba^{135} and Ba^{137}, which we have also studied, are included in this table for completeness. The results from these isotopes will be given in a subsequent paper.

Excitation energies of the levels populated in the reactions on the even-mass targets are given in Fig. 2 and in column 1 of Tables III–VII. The errors in the excitation energies are estimated to be ±5 keV up to about $E_x = 0.5$ MeV, ±10 keV for $0.5 \text{ MeV} < E_x < 2$ MeV, and ±10–20 keV above $E_x = 2$ MeV.

The orbital angular momentum l transferred by the captured neutron to the final state is given in column 2 of Tables III–VII. These l values are obtained by fitting the experimental angular distributions with DWBA curves (calculated with cutoff, as explained in Sec. IV). Many examples of these distributions and their fits are given in Figs. 3–7. Some spins and parities J^π of the final states are given in column 3 of Tables III–VII; their assignments are discussed in Sec. VA.

Tables III–VII also contain (column 4) the cross sections at the maxima of the angular distributions. These maxima are, in general, those taken from the DWBA curves which fit the experimental angular distributions (Figs. 3–7). For $l = 2$ transitions, the height of the first maximum (around 25°) is given in column 4 of Tables III–VII, although occasionally (as in Fig. 5) there are higher experimental points around 50°. However, for $l = 1$ distributions of $Ba^{138}(d,p)Ba^{139}$ at $E_x \geq 2.132$ MeV, the highest experimental points (around 50°) are given in column 4 of Tables III–VII, because this second maximum seems to be consistently higher and is not even qualitatively reproduced by the DWBA curves (as is seen in Fig. 4).

The absolute differential cross section for the

TABLE III. Summary of results from the $Ba^{138}(d,p)Ba^{139}$ reaction. The values for $(2J+1)S$ were obtained by use of DWBA calculations (zero-range approximations and local potentials) without cutoff (column 5) and with cutoff (column 6). The bound-state neutron well had the radius $r_n = 1.20$ F and the diffuseness $a_n = 0.703$ F.

E_x (MeV)	l	J^π	$(d\sigma/d\Omega)_{exp}^{max}$ (mb/sr)	$(2J+1)S$ No cutoff	$(2J+1)S$ Cutoff
0.0	3	$7/2^-$	3.8	4.15	5.6
0.630	1	$3/2^-$	4.0	0.98	1.29
1.084	1	$1/2^-$	1.6	0.43	0.53
1.284	5	$9/2^-$	0.30	4.4	5.4
(1.293)[a]		$(1/2, 3/2)$[a]	(<~0.1)		
1.422	3	$5/2^-$	1.05	1.00	1.23
1.543	5	$9/2^-$	0.26	3.6	4.3
1.625	(5)	$(9/2^-)$	~0.14	(~2.0)	(~2.3)
1.682	3		0.54	0.48	0.56
1.700	3	$(5/2^-)$	0.75	0.68	0.81
1.750			~0.41		
1.898			~0.27		
1.934			~0.36		
1.952			~0.24		
2.112			~0.33		
2.132	1		1.6	(0.48)[b]	(0.45)[b]
2.162	1		0.66	(0.20)	(0.19)
2.187	1		0.93	(0.28)	(0.27)
2.308	(3)		0.17	(0.13)	(0.15)
2.368			(0.38)		
2.381			~0.3		
2.439	1		0.57	(0.16)	(0.16)
2.484	1		1.38	(0.40)	(0.40)
2.534			~0.1		
(2.553)	(3)		(~0.14)	(~0.1)	(~0.11)
2.574	1		0.29	(0.09)	(0.09)
(2.675)					
(2.751)					
2.806			0.38		
2.857	(1)		0.17	(0.05)	(0.05)
2.909			~0.2		
2.939			~0.2		
3.007			~0.3		
3.035	(1)		0.25	(0.07)	(0.07)
(3.110)					
3.175	(1)		0.29	(0.08)	(0.08)
(3.192)					
3.221	1		0.43	(0.12)	(0.12)
(3.264)					
(3.285)					
3.293			~0.3		
(3.352)					
3.392	1		0.36	(0.1)	(0.1)
3.409	3		0.92	0.54	0.57
3.480	(3)		~0.5	(~0.29)	(~0.31)
(3.495)					
(3.516)					
(3.542)					
(3.579)					
(3.614)					
(3.675)					

[a] A level at $E_x = 1.2926$ MeV with $J = (\frac{1}{2}, \frac{3}{2})$ is suggested in Ref. 39.

[b] The angular distributions for the $l = 1$ levels at $E_x \geq 2.132$ MeV could not be fitted satisfactorily by DWBA curves (as seen in Fig. 4). This poor fit introduced an additional ±20% uncertainty in the values of $(2J+1)S$, which are therefore given in parentheses.

TABLE IV. Summary of results from the $Ba^{136}(d,p)Ba^{137}$ reaction. The values for $(2J+1)S$ were obtained by use of DWBA calculations (zero-range approximations and local potentials) without cutoff (column 5) and with cutoff (column 6). The bound-state neutron potential well had the radius $r_n = 1.20$ F and the diffuseness $a_n = 0.701$ F.[a]

E_x (MeV)	l	J^π	$(d\sigma/d\Omega)_{exp}{}^{max}$ (mb/sr)	$(2J+1)S$ No cutoff	$(2J+1)S$ Cutoff
0.0	2	$3/2^+$	0.42	0.68	0.74
0.281	0	$1/2^+$	0.93[b]	0.18	0.26
0.659[c]		$11/2^-$[a,c]	~0.03	~0.6	~0.9
(0.907)[d]			(≤0.004)		
(1.044)[e]			(≤0.002)		
1.292		$5/2^+$[a]	0.05		
1.462		$5/2^+$[a]	~0.04		
1.794	3	$7/2^-$	2.5	2.9	4.0
1.839	0	$1/2^+$[a]	(~0.02)[b]		
(1.857)	(0)	$(1/2^+)$	(~0.03)[b]		
1.903		$5/2^+$[a]	~0.01		
2.041		$5/2^+$[a]	~0.01		
2.180	1	$3/2^-$	3.2	0.79	1.06
2.268			~0.03		
2.663	1	$1/2^-$	1.08	0.28	0.36
2.704			~0.05		
(2.810)	(3)		(~0.18)	(~0.19)	(~0.25)
2.848	3		0.13	0.14	0.18
2.875	3		0.22	0.23	0.29
2.911	3		0.18	0.18	0.23
3.008			~0.03		
(3.041)			(~0.02)		
3.141	5	$9/2^-$	0.25	3.8	4.8
3.228[f]	3		0.31	0.31	0.38
3.254			~0.09		
3.319	1		~0.45	~0.12	~0.15
3.332	3	$(5/2^-)$	0.98	1.00	1.22
3.407	1		0.60	0.15	0.19
3.496[g]	3[g]		0.28[g]	0.27[g]	0.32[g]
3.591	3		0.17	0.16	0.19
(3.606)			(~0.03)		
3.640	3		0.45	0.42	0.50
3.684	1		0.29	0.08	0.09
3.703	3		0.21	0.19	0.22
3.723			0.08		
3.782	–[h]		(~0.3)		
3.805	(1)[h]		(~0.19)	(~0.05)	(~0.06)
3.827	3		0.33	0.30	0.35

[a] In their studies of the $Ba^{138}(p,d)Ba^{137}$, Bruge *et al.* (Ref. 44) observed the following levels: $E_x = 0.0$ MeV $[\frac{3}{2}^+]$, 0.281 $[\frac{1}{2}^+]$, 0.662 $[\frac{11}{2}^-]$, 1.294 $[\frac{5}{2}^+]$, 1.465 $[\frac{5}{2}^+]$, 1.838 $[\frac{1}{2}^+]$, 1.900 $[\frac{5}{2}^+]$, 2.042 $[\frac{5}{2}^+]$, 2.236 $[\frac{1}{2}^+]$, 2.335 $[\frac{11}{2}^-]$, 2.53, 2.67, 2.75, 2.89, 2.99 $[\frac{11}{2}^-]$, and 3.20. The lowest $\frac{1}{2}^+$ and $\frac{11}{2}^-$ levels are observed to be much more strongly excited than the other levels of these spins and parities. No l values could be assigned in the present investigation to $\frac{11}{2}^-$ and $\frac{5}{2}^+$ levels of Ba^{137}.

[b] At $\theta_{lab} = 5°$.

[c] Reference 43 lists this level at $E_x = 0.6616$ MeV, $J^\pi = \frac{11}{2}^-$.

[d] Reference 1 lists this level at $E_x = 0.90$ MeV.

[e] Reference 43 lists this level at $E_x = 1.05$ MeV.

[f] This and all higher levels may be due to unknown states above $E_x \approx 5.0$ MeV in Ba^{138} from the (d,p) reaction on the contaminant Ba^{137}.

[g] The shape of the angular distribution suggests that a contribution in addition to $l = 3$ may be significant at large angles (as seen in Fig. 6). If it is an unresolved $l = 5$ distribution, then $(d\sigma/d\Omega)_{exp}{}^{max} \approx 0.06$ mb/sr and hence $S_{cutoff} \approx 0.1$ for an assumed $J^\pi = \frac{9}{2}^-$ state. Separating out this contribution would decrease the given values for the peak cross section and the spectroscopic factor of the $l = 3$ level only by about 10–15%. The small contribution from the contaminant $l = 5$ level at $E_x = 1.284$ MeV in Ba^{139} from the $Ba^{138}(d,p)$ reaction cannot account for the major part of the underlying $l = 5$ shape and has been substracted out.

[h] Incomplete data.

ground-state reaction, $Ba^{138}(d,p_0)Ba^{139}$ at $\theta_{lab}=40°$, was determined to be $d\sigma/d\Omega=3.55\pm0.2$ mb/sr. For the other isotopes, the absolute differential cross sections were determined to ±10%. The errors in relative cross sections within any one isotope are ±5%.

In general, the exposure times in the spectrograph limited the detected levels to those with

TABLE V. Summary of results from the $Ba^{134}(d,p)Ba^{135}$ reaction. The values for $(2J+1)S$ were obtained by use of DWBA calculations (zero-range approximations and local potentials) without cutoff (column 5) and with cutoff (column 6). The bound-state neutron potential well had the radius $r_n=1.20$ F and the diffuseness $a_n=0.699$ F.[a]

E_x (MeV)	l	J^π	$(d\sigma/d\Omega)_{exp}^{max}$ (mb/sr)	$(2J+1)S$ No cutoff	$(2J+1)S$ Cutoff
0.0	2	$3/2^+$	0.80	1.31	1.38
0.221	0	$1/2^+$	1.56[b]	0.30	0.41
0.269		$11/2^-$[a]	(~0.08)		
(0.487)	2[a]		(~0.02)		
(0.594)			(~0.01)		
0.717			~0.05		
(0.855)			(~0.02)		
0.909	0	$1/2^+$	0.19[b]	0.035	0.047
0.979	2		0.27	0.36	0.35
1.215			~0.02		
1.445	3	$7/2^-$	2.0	2.55	3.6
1.581	1	$3/2^-$	3.1	0.82	1.12
1.876			~0.04		
1.972			~0.03		
1.997	1	$1/2^-$	0.78	0.21	0.28
2.076	(1)		0.06	(0.016)	(0.021)
2.118			~0.03		
2.152	(3)		0.2	(0.24)	(0.32)
2.447	1		0.28	0.073	0.094
2.478	(3)		0.14	(0.16)	(0.21)
2.568[c]			~0.19		
2.603			~0.11		
2.663			~0.06		
(2.686)			(~0.02)		
2.709	(1)		~0.22	(0.06)	(0.07)
2.728	1		0.66	0.17	0.22
2.784	(1)		~0.14	(0.035)	(0.045)
2.850	3		0.37	0.37	0.48
(2.874)			(~0.15)		
2.899			0.23		
2.949	3		0.51	0.51	0.64
3.085	1		1.09	0.27	0.36
(3.327)[d]			(~0.08)		
3.630			~0.15		
(3.670)			(~0.2)		
3.787			~0.3		
3.936[e]			~0.2		
4.074			~0.1		
4.269			~0.2		
(4.729)			(~0.1)		
4.890			~0.2		
4.940			~0.1		

[a] Reference 43 lists levels at $E_x=0.0$ MeV $[\frac{3}{2}^+]$, 0.218 $[(\frac{1}{2}^+)]$, 0.268 $[\frac{11}{2}^-]$, 0.481 $[l=2]$, 0.586, and 0.862. Except for the ground state and first excited state, no values for l and J^π could be assigned to these levels in the present investigation.

[b] At $\theta_{lab}=5°$.

[c] This and all higher levels may be due to unknown states above $E_x\approx4.7$ MeV in Ba^{136} from the (d,p) reaction on the contaminant Ba^{135}.

[d] This and all higher levels may be due to unknown states above $E_x\approx5.0$ MeV in Ba^{138} from the (d,p) reaction on the contaminant Ba^{137}.

[e] This and all higher levels may be due to unknown states above $E_x\approx3.9$ MeV in Ba^{137} from the (d,p) reaction on the contaminant Ba^{136}.

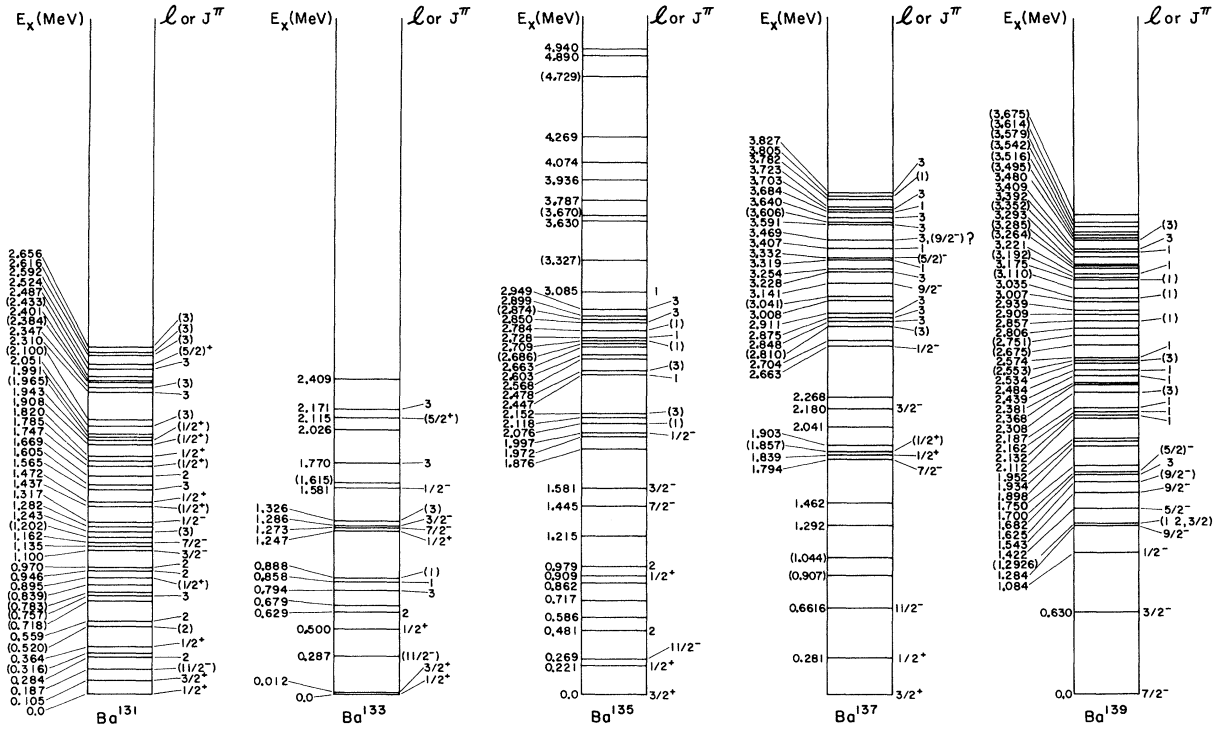

FIG. 2. Excited states of the odd-A isotopes of Ba, as observed in the (d,p) reaction. Additional information on spins and excitation energies are included where available. Further information on Ba^{137} levels obtained from the (p,d) reaction (Ref. 44) is given in a footnote to Table IV.

TABLE VI. Summary of results from the $Ba^{132}(d,p)Ba^{133}$ reaction. The values for $(2J+1)S$ were obtained by use of DWBA calculations (zero-range approximations and local potentials) without cutoff (column 5) and with cutoff (column 6). The bound-state neutron potential well had the radius $r_n = 1.20$ F and the diffuseness $a_n = 0.696$ F.

E_x (MeV)	l	J^π	$(d\sigma/d\Omega)_{\exp}{}^{\max}$ (mb/sr)	$(2J+1)S$ No cutoff	$(2J+1)S$ Cutoff
0.0 [a]	0	$1/2^+$	1.7 ± 0.3 [b]	~0.36	~0.45
0.012 [a]	2	$3/2^+$	0.69 ± 0.08	~1.20	~1.23
(0.294) [c]		$(11/2^-)$ [c]	(~0.2)		
0.500	0	$1/2^+$	~0.11 [b]	~0.02	~0.03
0.629	2		0.23	0.35	0.33
0.679			~0.03		
0.794	3		0.15	0.24	0.36
0.858	1		0.36	0.11	0.15
0.888	(1)		~0.1	(~0.03)	(~0.04)
1.247	0	$1/2^+$	~0.35 [b]	~0.07	~0.08
1.273 [a]	3	$7/2^-$	1.4 ± 0.2	~1.95	~2.9
1.286 [a]	1	$3/2^-$	2.3 ± 0.3	~0.66	~0.89
1.326	(3)		0.13	(0.19)	(0.28)
1.581	1	$1/2^-$	0.71	0.21	0.28
(1.615)			(~0.04)		
1.770	3		0.25	0.34	0.48
2.026			~0.1		
2.115	(2)	$(5/2^+)$	~0.1	(~0.11)	(~0.11)
2.171	3		~0.05	~0.06	~0.09
2.409			~0.2		

[a] Incompletely resolved.
[b] At $\theta_{lab} = 5°$.
[c] Reference 43 lists this level at $E_x = 0.287$ MeV $[(\frac{11}{2}^-)]$. No l value could be assigned in the present investigation.

peak cross sections greater than 0.2 mb/sr for the Ba^{139} spectrum, 0.02 mb/sr for the spectra of Ba^{137} and Ba^{135}, 0.1 mb/sr for the Ba^{133} spectrum, and 0.05 mb/sr for the Ba^{131} spectrum. The relatively high limit for Ba^{139} is due to shorter exposure times. The limits for Ba^{133} and Ba^{131} do not fully reflect the low isotopic enrichments of these targets, which may result in some levels being completely obscured. Contributions from the spectra of the contaminating barium isotopes (Table I),

TABLE VII. Summary of results from the $Ba^{130}(d,p)Ba^{131}$ reaction. The values for $(2J+1)S$ were obtained by use of DWBA calculations (zero-range approximations and local potentials) without cutoff (column 5) and with cutoff (column 6). The bound-state neutron potential well had the radius $r_n = 1.20$ F and the diffuseness $a_n = 0.694$ F.[a]

E_x (MeV)	l	J^π	$(d\sigma/d\Omega)_{exp}^{max}$ (mb/sr)	$(2J+1)S$ No cutoff	$(2J+1)S$ Cutoff
0.0	0	$1/2^+$	2.4[b]	0.53	0.61
0.105	2	$3/2^+$	0.56	1.03	0.99
(0.187)[c]		$(11/2^-)$[c]	(0.002)		
0.284	2		0.24	0.43	0.42
(0.316)			(~0.04)		
0.364	0	$1/2^+$	0.08[b]	0.016	0.019
(0.520)	(2)		(0.12)	(0.20)	(0.20)
0.559	2		0.30	0.51	0.48
(0.718)			(~0.03)		
0.757	3		0.21	0.35	0.51
(0.783)			(~0.04)		
(0.839)			(~0.007)		
0.895	(0)	$(1/2^+)$	(0.05)[b]	(0.01)	(0.012)
0.946	2		0.11	0.17	0.16
0.970	2		0.15	0.22	0.21
1.100	1	$3/2^-$	2.1	0.62	0.84
(1.135)			(~0.06)		
1.162	3	$7/2^-$	0.80	1.19	1.73
(1.202)			(~0.02)		
1.243	(3)		(~0.05)	(~0.07)	(~0.11)
1.282			~0.04		
1.317	1	$1/2^-$	0.49	0.16	0.21
1.437	(0)	$(1/2^+)$	(0.04)[b]	(0.008)	(0.009)
1.472	0	$1/2^+$	0.10[b]	0.018	0.022
1.565	3		0.22	0.34	0.48
1.605			~0.04		
1.669	2		0.067	0.09	0.08
1.747	(0)	$(1/2^+)$	(~0.04)[b]	(~0.008)	(~0.009)
1.785			~0.04		
1.820	0	$1/2^+$	0.26[b]	0.049	0.057
1.908	(0)	$(1/2^+)$	0.28[b]	(0.052)	(0.062)
1.943	(0)	$(1/2^+)$	~0.06[b]	(0.011)	(0.013)
(1.965)			(~0.05)		
1.991			~0.09		
2.051	(3)		~0.04	(~0.06)	(~0.08)
(2.100)			(~0.1)		
2.310	3		0.08	0.11	0.15
2.347	(3)		0.04	0.06	0.08
(2.384)			(~0.15)		
2.401			~0.25		
(2.433)			(~0.08)		
2.487	3		0.21	0.28	0.38
2.524	2	$(5/2^+)$	0.48	0.50	0.44
2.592	(3)		0.11	(0.14)	(0.19)
2.616	(3)		0.10	(0.13)	(0.17)
2.656	(3)		0.14	(0.18)	(0.24)

[a] Reference 43 lists levels at $E_x = 0.0$ MeV $[(\frac{1}{2}^+)]$, 0.115, 0.285, 0.364, 0.536, 0.882, 0.990, 1.204.

[b] At $\theta_{lab} = 5°$.

[c] J. M. D'Auria, H. Bakhru, and I. L. Preiss [Phys. Rev. 172, 1176 (1968)] list this level at $E_x = 0.187$ MeV with $J^\pi = (\frac{11}{2}^-)$. No l value could be assigned in the present investigation.

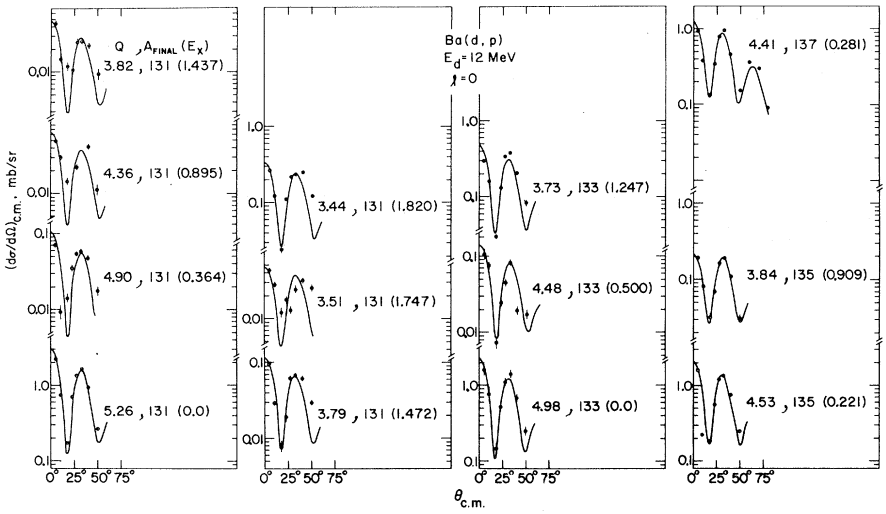

FIG. 3. Measured angular distributions of the Ba(d,p) reactions with $l=0$ angular-momentum transfer. Each distribution is labeled with the mass A_{FINAL} of the residual barium nucleus, the Q value (MeV) for the reaction, and the excitation energy E_x (MeV) of the states. The curves represent zero-range local DWBA calculations with a cutoff radius at about the nuclear surface. Larger-than-average errors can arise from uncertainties generated by unresolved levles and by background subtraction.

including those of the $Ba^{135}(d,p)Ba^{136}$ and $Ba^{137}(d,p)Ba^{138}$ reactions were subtracted to yield the values given in the tables.

In general, the present study was limited to excitation energies below 3 MeV; the exact limits are indicated by arrows in Fig. 10. In the case of $Ba^{134}(d,p)Ba^{135}$, this limit was extended to 5 MeV to test the usefulness of the (d,p) reaction at these higher excitation energies; a number of levels were identified but no l values could be assigned beyond $E_x=3.085$ MeV (Table V). In the Ba^{139} spectrum, a number of weak levels seen above the limit of systematic data evaluation at $E_x=3.480$ MeV are included in Table III and Fig. 2.

IV. DISTORTED-WAVE ANALYSIS

The DWBA analysis of our data was performed in the usual way[24] with Woods-Saxon potentials[25] and the code JULIE.[26] Unless otherwise noted,

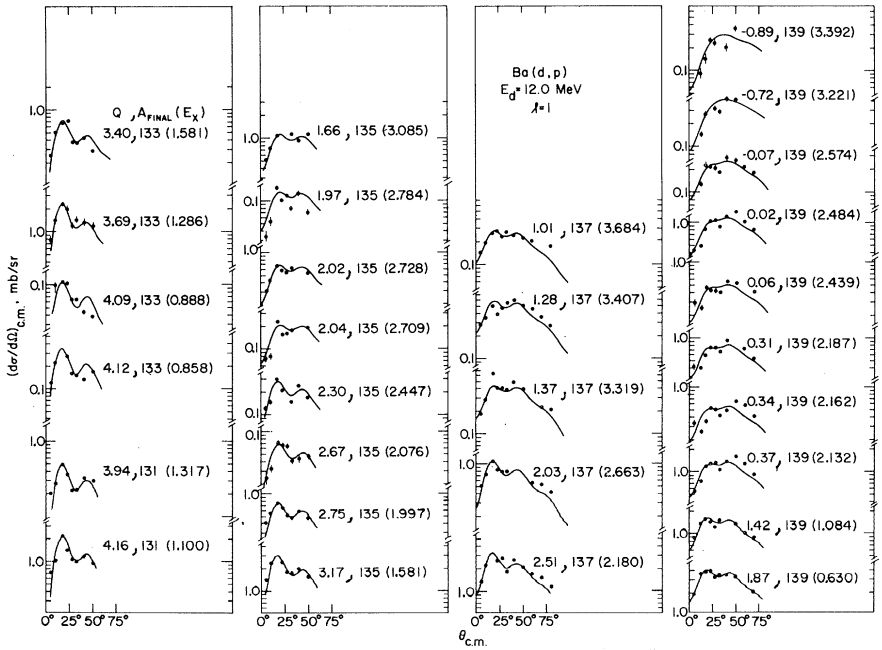

FIG. 4. Measured angular distributions of the Ba (d,p) reactions with $l=1$ angular-momentum transfer. The details are as described for Fig. 3.

the deuteron and proton optical parameters given in Table VIII were used; they are essentially those published by Wiedner, Heusler, Solf, and Wurm.[4]

A. Extraction of Spectroscopic Factors

The calculations to extract a basic set of spectroscopic factors were done with the zero-range approximation and local potential (ZRL); finite-range and nonlocality corrections will be discussed in Sec. IVC. In most cases, the angular distributions calculated with a lower cutoff[27] at $r \approx 1.25\ \mathrm{F} \times A^{1/3}$ fitted our measured angular distributions much better than did those calculated without cutoff, as is demonstrated for several examples in Fig. 8. The over-all normalization factor of the cross section calculated by DWBA analysis[28] was 1.65 (assuming a deuteron wave function from a Gartenhaus potential). Spin-orbit interactions were included in the proton, deuteron, and neutron potentials. The strength of the spin-orbit poten-

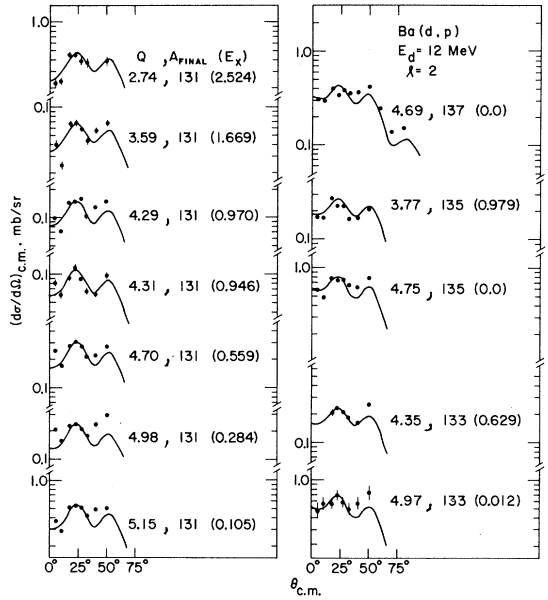

FIG. 5. Measured angular distributions of the Ba(d,p) reactions with $l=2$ angular momentum transfer. The details are as described for Fig. 3.

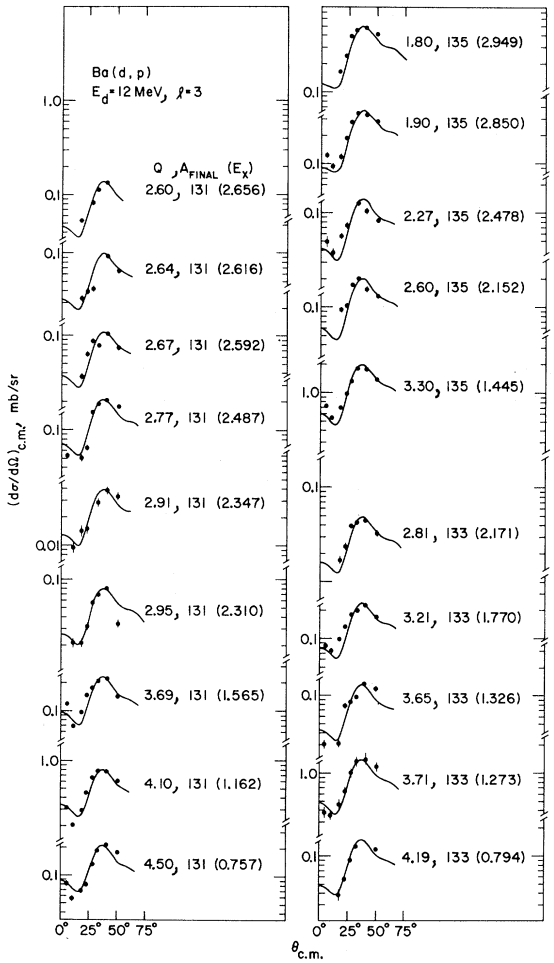

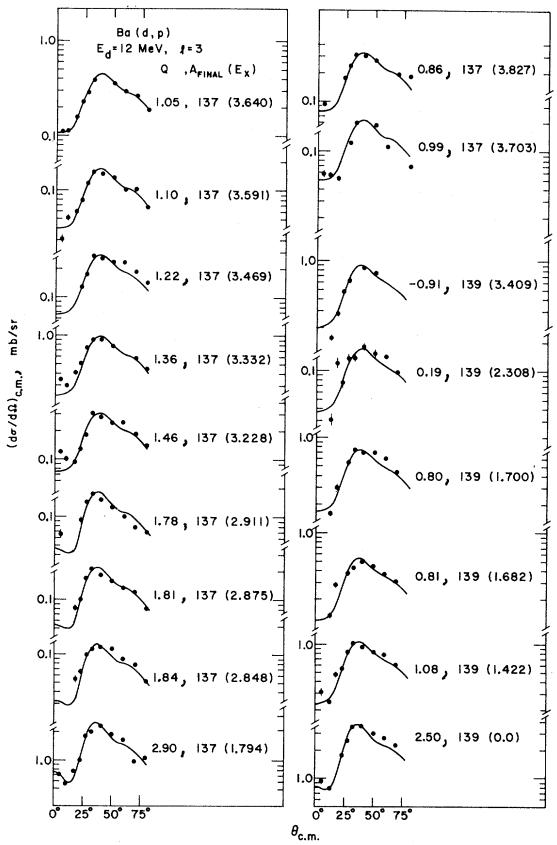

FIG. 6. Measured angular distributions of the Ba(d,p) reactions with $l=3$ angular momentum transfer. The details are as described for Fig. 3.

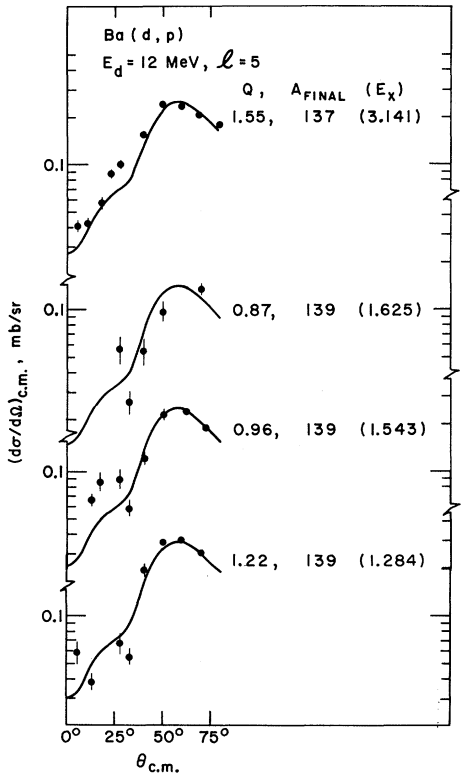

FIG. 7. Measured angular distributions of the Ba(d,p) reactions with $l=5$ angular momentum transfer. The details are as described for Fig. 3.

tial for the neutron was taken to be 16.0 times the Thomas value. For the levels without J assignment, the DWBA cross section was obtained by averaging the values for $J=l+\frac{1}{2}$ and $J=l-\frac{1}{2}$.

The spectroscopic factor S was obtained in the usual manner by comparing the experimental maximum[29] differential cross section $(d\sigma/d\Omega)_{\text{exp}}^{\text{max}}$ of the angular distributions with the calculated maximum $(d\sigma/d\Omega)_{\text{DWBA}}^{\text{max}}$, i.e., by use of the relation

$$(d\sigma/d\Omega)_{\text{exp}}^{\text{max}}/(d\sigma/d\Omega)_{\text{DWBA}}^{\text{max}}=(2J+1)S, \qquad (1)$$

where J is the spin of the final state. All data were analyzed with the bound-state neutron radius $r_n=1.20$ F and the diffuseness[30] $a_n\approx 0.70$ F. The results of this analysis are given in Tables III – VII in column 5 for the DWBA calculations without lower cutoff, and in column 6 for the calculations with lower cutoff.

A few cases were computed with a set of deuteron and proton parameters different from those in Table VIII, namely, those extrapolated from the values given as family B by Perey and Perey.[31,32] With these parameters, the spectroscopic factors (obtained for selected levels) were increased. These increases ranged from 6% (for $l=5$) to 40% (for $l=0$) for calculations with cutoff; for calculations without cutoff the corresponding increases ranged from 20 to 70%.

B. Effects of the Geometric Parameters of the Bound-State Potential Well

The parameters of the potential well of the neutron bound state are not accurately known. Hence we have investigated the dependence of the extracted spectroscopic factors S on these parameters. The values of S extracted in Sec. IVA (with a neutron well radius $r_n=1.20$ F and diffuseness $a_n\approx 0.70$ F) and given in Tables III – VII will be taken as a basis for the comparisons.

In general, if either r_n or a_n is increased, the bound-state wave function extends to larger radii and S is decreased. It was pointed out by Sharpey-Schafer,[17,18] that the variation in S is reduced if r_n and a_n are simultaneously varied in such a way that the rms radius of the potential well is kept constant. For a Woods-Saxon potential well with half-way radius $r_nA^{1/3}$ and diffuseness a_n, the mean-square radius $\langle R^2\rangle$ is given to a good approximation by the expression[33]

$$\langle R^2\rangle=\tfrac{3}{5}(r_nA^{1/3})^2+\tfrac{7}{5}\pi^2a_n^2. \qquad (2)$$

Values of S for 13 selected levels ($l=0$, 1, 2, 3, and 5) extracted with various combinations of r_n and a_n are compared in Table IX. Both cutoff and no-cutoff values are given. The values of S_{abs} are calculated with the "standard" parameters $r_n=1.20$ F and $a_n\approx 0.70$ F (these parameters yield $g\equiv\langle R^2\rangle^{1/2}/A^{1/3}\approx 1.06$ F) and appear in column 6. Columns 9 and 10 give values of S calculated with the same g, but with $r_n=1.15$ and 1.25 F, respectively. Columns 7 and 8 and columns 10 and 11 give values of

TABLE VIII. Deuteron and proton DWBA parameters for Ba(d,p) at $E_d=12$ MeV. The symbols are as usual: V = real volume potential, W_D = imaginary derivative surface-absorption potential, V_{so} = spin-orbit potential, r_0 = real radius, r_0' = imaginary radius, r_C = Coulomb radius, a_S = real diffuseness, a_D' = imaginary diffuseness, E_p = energy (MeV) of outgoing protons.

	V (MeV)	W_D (MeV)	V_{so} (MeV)	r_0 (F)	r_0' (F)	r_C (F)	a_S (F)	a_D' (F)
d	100	13.0[a]	5.0	1.18	1.34	1.18	0.8	0.68
p	V_p[b]	10.0	4.5	1.25	1.20	1.25	0.67	0.69

[a] Reference 4 specifies (14.0 ± 2.5) MeV.

[b] The potential V_p (in MeV) is given by

$$V_p=50.3+32.4\,\frac{N-Z}{A}+0.4\,\frac{Z}{A^{1/3}}-0.4E_p\,.$$

The factor 32.4 in the second term on the right in this equation is from the abstract and report of work prior to publication of Ref. 4; the value 42.3 given in Sec. 3.4 of Ref. 4 is presumably a misprint.

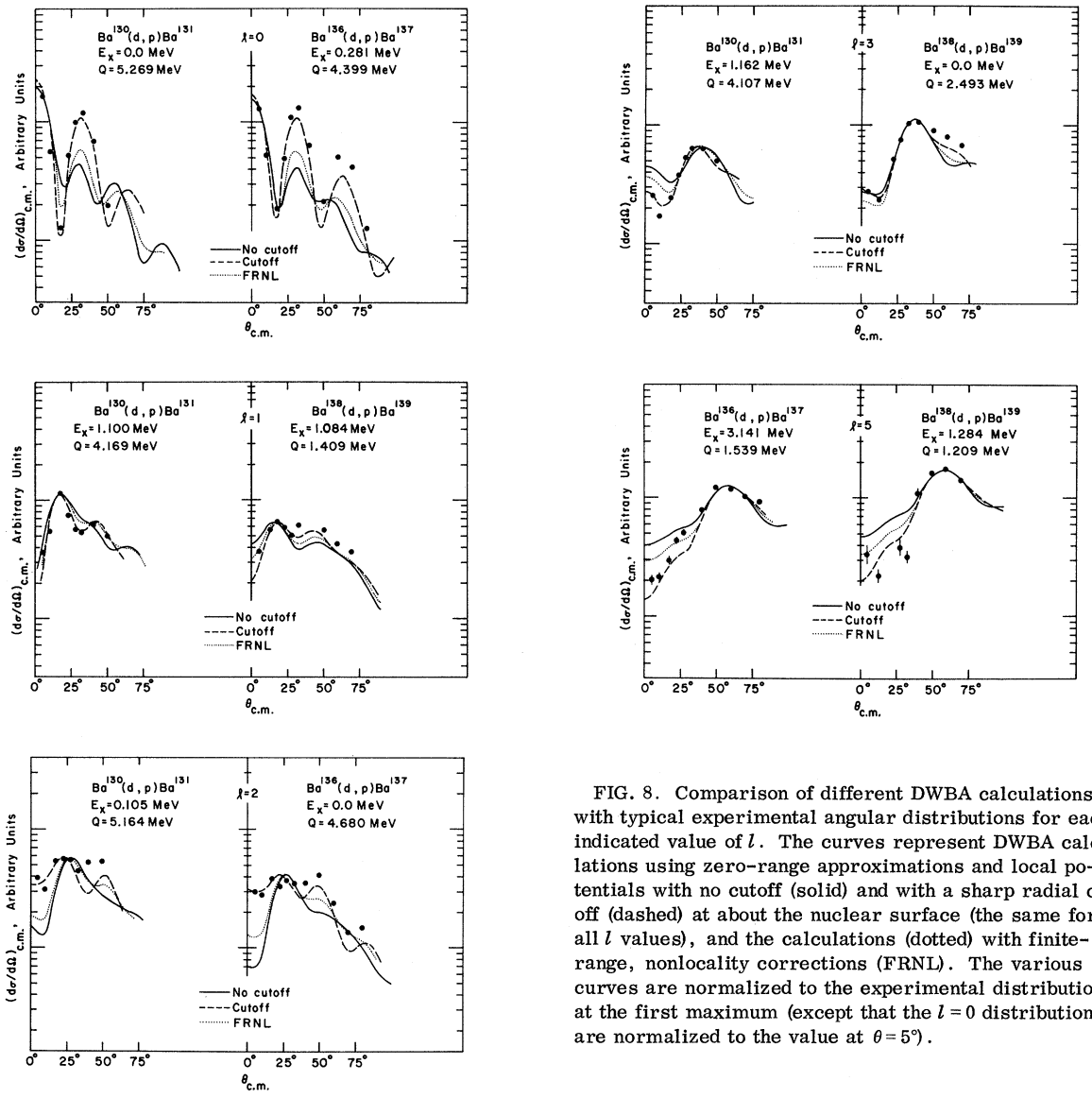

FIG. 8. Comparison of different DWBA calculations with typical experimental angular distributions for each indicated value of l. The curves represent DWBA calculations using zero-range approximations and local potentials with no cutoff (solid) and with a sharp radial cutoff (dashed) at about the nuclear surface (the same for all l values), and the calculations (dotted) with finite-range, nonlocality corrections (FRNL). The various curves are normalized to the experimental distributions at the first maximum (except that the $l=0$ distributions are normalized to the value at $\theta=5°$).

S calculated with $g \approx 1.02$ and 1.09, respectively. Values of S are given as ratios to the corresponding S_{abs}.

Table IX shows that for $l=0-3$, S varies only ~5% when r_n and a_n are varied with the rms radius of the potential well kept constant. Table IX also shows that the $l=5$ transitions are more sensitive to the parameters of the bound-state well. Even with a constant rms radius, the value of S for $l=5$ varies more than twice as much as for the lower l values. The dependence of S on g for the sample levels is exhibited in Fig. 9 for both cutoff and no-cutoff calculations, the dependence in the former case being slightly greater than that in the latter. Thus for all l values, the value of S is very sensitive to changes in the rms radius.

It is of interest to explore the generality of the reduced variation in S for a constant rms radius. It has been previously noted, e.g., in (d,t) and (d, He^3) reactions,[34] that the DWBA cross section for any given state is nearly proportional to the square of the amplitude of the asymptotic tail of the bound-state wave function. In the present (d,p) study with 12-MeV deuterons, this proportionality is again found to hold for all l values. It is especially accurate (±2%) for cutoff calculations (as expected since the interior contribution has been cut out); but the relationship is also found to be valid (within ±8%) for no-cutoff calculations, although in most cases the inclusion of the nuclear interior sizeably increases the DWBA cross section (Table IX). It appears therefore that the reduced varia-

tion in S for a constant rms radius in the case of low l values must be due to specific properties of the Woods-Saxon well shape, which gives the same magnitude for the tail of the wave function for constant rms radius in these cases. As the centrifugal barrier increases, the correlation decreases; i.e., for $l=5$ transitions the normalization of the tail and the spectroscopic factor depends more on r_n and less on a_n. Although the relationship between the rms radius of the bound-state well and the spectroscopic factor may be empirically useful, it lacks general applicability.

C. Effects of Finite Range and Nonlocality

The effects of the finite range of the proton-neutron interaction and the nonlocality of the optical-model potentials were also investigated. Both of these effects were included in the local-energy approximation by using a standard procedure which was recently used, for example, by Hiebert, Newman, and Bassel.[35] In this approximation, both effects reduce to damping factors which multiply the ZRL form factor before its use in the distorted-wave calculation. Because of uncertainties in determination of nonlocality parameters for bound states[36,37] this correction was applied to the scattering channels only.

The nonlocality parameters β have been previously determined from the energy dependence of the optical potentials: $\beta \approx 0.54$ for deuterons and $\beta \approx 0.85$ F for the protons.[35] The range parameter for the (d,p) reaction obtained with the Hulthén wave function of the deuteron is $R \approx 1.25$ F.[38] With these parameters and the optical potentials given in Table VIII, the corrected form factor varies smoothly from $\sim 0.6u(r)$ in the nuclear interior to $1.02u(r)$ outside the nucleus, $u(r)$ being the uncorrected single-particle bound-state wave function used in the ZRL calculation.

TABLE IX. Spectroscopic factors for several typical transitions. They were obtained by use of DWBA calculations (zero-range approximations and local potentials) without and with cutoff. Column 6 gives the absolute spectroscopic factors S_{abs} for the radius $r_n = 1.20$ F and the diffuseness $a_n \approx 0.70$ F of the bound-state neutron potential well. Columns 7–12 give values of the spectroscopic factors relative to S_{abs} for the indicated combinations of r_n and a_n.[a] They are grouped according to the corresponding rms radius of the bound-state neutron potential well [Eq. (2)]. The unchanged rms radius of columns 9 and 10 is the same as that used to compute S_{abs}.

Target isotope	Excitation energy (MeV)	Q (MeV)	J^π		S_{abs}	$S(r_n;a_n)/S_{abs}$ 3.2% smaller rms radius		Unchanged rms radius		3.2% larger rms radius	
					$r_n=1.20$ F $a_n\approx 0.70$ F	$r_n=1.15$ F $a_n\approx 0.70$ F	1.20 F ≈0.59 F	1.15 F ≈0.79 F	1.25 F ≈0.59 F	1.20 F ≈0.79 F	1.25 F ≈0.70 F
Ba^{130}	0.0	5.27	$\frac{1}{2}^+$	no cutoff	0.27	1.11	1.22	0.96	1.08	0.85	0.88
				cutoff	0.31	1.23	1.26	1.01	1.02	0.83	0.81
Ba^{136}	0.281	4.40	$\frac{1}{2}^+$	no cutoff	0.09	1.07	1.18	0.94	1.09	0.87	0.91
				cutoff	0.13	1.22	1.27	1.00	1.02	0.83	0.81
Ba^{130}	1.100	4.17	$\frac{3}{2}^-$	no cutoff	0.16	1.13	1.22	0.97	1.06	0.87	0.89
				cutoff	0.21	1.22	1.30	1.01	1.06	0.83	0.83
Ba^{134}	1.997	2.75	$\frac{1}{2}^-$	no cutoff	0.11	1.10	1.19	0.97	1.08	0.87	0.89
				cutoff	0.14	1.21	1.30	0.99	1.08	0.83	0.84
Ba^{138}	0.630	1.86	$\frac{3}{2}^-$	no cutoff	0.25	1.11	1.18	0.97	1.08	0.89	0.91
				cutoff	0.32	1.17	1.26	0.97	1.06	0.83	0.85
Ba^{138}	1.084	1.41	$\frac{1}{2}^-$	no cutoff	0.22	1.10	1.17	0.96	1.07	0.87	0.90
				cutoff	0.27	1.18	1.27	0.98	1.06	0.84	0.85
Ba^{130}	0.105	5.16	$\frac{3}{2}^+$	no cutoff	0.26	1.12	1.17	0.98	1.03	0.85	0.84
				cutoff	0.25	1.28	1.28	1.05	1.00	0.83	0.79
Ba^{134}	0.0	4.75	$\frac{3}{2}^+$	no cutoff	0.33	1.15	1.21	1.00	1.05	0.87	0.85
				cutoff	0.35	1.30	1.29	1.05	1.00	0.84	0.78
Ba^{136}	0.0	4.68	$\frac{3}{2}^+$	no cutoff	0.17	1.15	1.22	1.00	1.04	0.86	0.85
				cutoff	0.19	1.29	1.29	1.04	1.00	0.83	0.79
Ba^{130}	1.162	4.11	$\frac{7}{2}^-$	no cutoff	0.15	1.18	1.19	1.02	1.01	0.86	0.84
				cutoff	0.22	1.29	1.31	1.04	1.00	0.81	0.77
Ba^{138}	0.0	2.49	$\frac{7}{2}^-$	no cutoff	0.52	1.20	1.22	1.03	1.03	0.86	0.85
				cutoff	0.70	1.30	1.31	1.04	1.02	0.82	0.79
Ba^{136}	3.141	1.54	$\frac{3}{2}^-$	no cutoff	0.38	1.40	1.24	1.14	0.89	0.82	0.72
				cutoff	0.48	1.46	1.33	1.14	0.91	0.80	0.70
Ba^{138}	1.284	1.21	$\frac{3}{2}^-$	no cutoff	0.44	1.41	1.24	1.13	0.89	0.82	0.72
				cutoff	0.54	1.45	1.31	1.12	0.90	0.79	0.70

[a] Actual values of a_n vary in such a manner that the rms radius $\langle R^2\rangle^{1/2}$ in Eq. (2) is proportional to $A^{1/3}$.

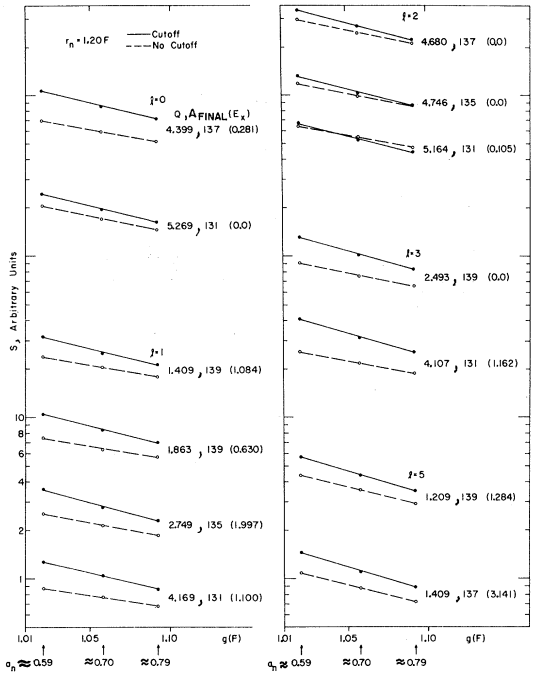

FIG. 9. Spectroscopic factors (in arbitrary units) calculated with and without cutoff for representative states of each l value as a function of the rms radius, expressed as the factor $g = \langle R^2\rangle^{1/2}/A^{1/3}$. Actual values of the spectroscopic factors can be obtained from Table IX. The bound-state radius was kept constant at $r_n = 1.20$ F. The approximate value of the bound-state diffuseness a_n corresponding to this radius is also indicated on the abscissa.

Spectroscopic factors resulting from finite-range nonlocal (FRNL) calculations for some typical states are given in column 7 of Table X; angular distributions are shown in Fig. 8. In general, the FRNL spectroscopic factors are between those from cutoff and no-cutoff ZRL calculations. *A priori*, the FRNL calculations have better theoretical justification and should be preferred. However, the angular distributions produced by the ZRL calculations with cutoff fit the experimental points significantly better than those from FRNL calculations. This may indicate that the present FRNL procedure still does not lead to sufficient damping of the form factor, as has been previously discussed by Parkinson *et al.*[34] The "correct" spectroscopic factors are probably between the FRNL and the ZRL values with cutoff. Nevertheless, as is seen from Table X, even the values of S computed with the extreme assumptions of cutoff and no cutoff are in reasonable agreement when one considers the uncertainties that may arise from the DWBA itself. And as has been noted above, a far greater variation in S can arise from arbitrariness in the choice of r_n and a_n.

V. DISCUSSION

A. General

Several studies of the $Ba^{138}(d,p)$ reaction have been reported previously.[1-5] All of these studies concur in a mean value $Q_0 = 2.494 \pm 0.005$ MeV for the reaction, which is in agreement with the very precise value $Q_0 = 2.499 \pm 0.001$ MeV derived from the recent study[39] of the $Ba^{138}(n,\gamma)$ reaction. With regard to the excited states of Ba^{139}, the present study is in very good agreement with the most ac-

TABLE X. Spectroscopic factors for some typical transitions. The results of the DWBA calculation with zero-range approximation and local potentials with cutoff (column 6) and without cutoff (column 8) are compared with the results obtained with finite-range and nonlocality corrections (FRNL; column 7). The bound-state potential well had the radius $r_n = 1.20$ F and the diffuseness $a_n \approx 0.70$ F.[a]

Target isotope	Excitation energy (MeV)	Q (MeV)	J^π	$(d\sigma/d\Omega)_{exp}^{max}$ (mb/sr)	Spectroscopic factors Cutoff	FRNL	No cutoff
Ba^{130}	0.0	5.27	$1/2^+$	2.4	0.31	0.28	0.27
Ba^{136}	0.281	4.40	$1/2^+$	0.93	0.13	0.10	0.09
Ba^{130}	1.100	4.17	$3/2^-$	2.1	0.21	0.17	0.16
Ba^{134}	1.997	2.75	$1/2^-$	0.78	0.14	0.12	0.11
Ba^{138}	0.630	1.86	$3/2^-$	4.0	0.32	0.27	0.25
Ba^{138}	1.084	1.41	$1/2^-$	1.6	0.27	0.23	0.22
Ba^{130}	0.105	5.16	$3/2^+$	0.56	0.25	0.27	0.26
Ba^{134}	0.0	4.75	$3/2^+$	0.80	0.35	0.34	0.33
Ba^{136}	0.0	4.68	$3/2^+$	0.42	0.19	0.18	0.17
Ba^{130}	1.162	4.11	$7/2^-$	0.80	0.22	0.18	0.15
Ba^{138}	0.0	2.49	$7/2^-$	3.8	0.70	0.58	0.52
Ba^{136}	3.141	1.54	$9/2^-$	0.25	0.48	0.41	0.38
Ba^{138}	1.284	1.21	$9/2^-$	0.30	0.54	0.47	0.44

[a]See Ref. 30.

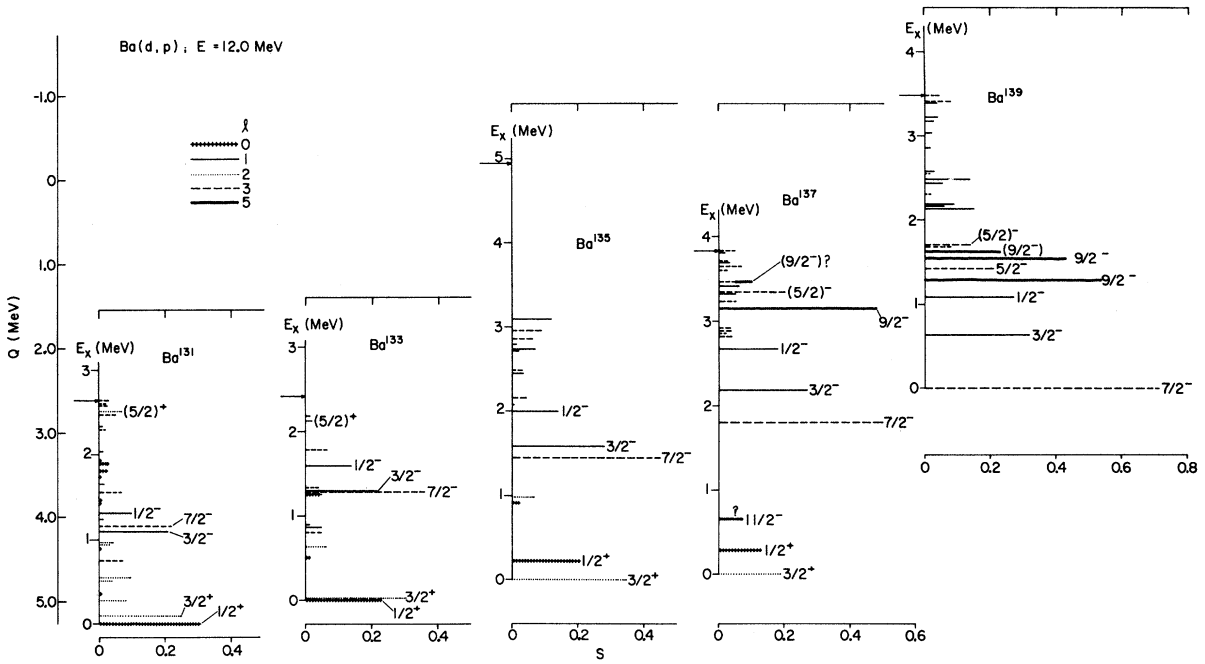

FIG. 10. Summary of spectroscopic information. The value of S is indicated by the length of the line plotted at the appropriate excitation energy E_x in the product nucleus and Q value in the Ba(d,p) reaction. The spectroscopic factors are those obtained from zero-range local DWBA calculations with cutoff and a bound-state neutron well of radius r_n = 1.20 F and diffuseness $a_n \approx 0.70$ F.

curate previous study of Rapaport and Kerman[5] up to the full excitation energy reported here (Table III). Where the levels are also seen in the (n,γ) reaction (up to 2.5 MeV), the two sets of (d,p) results bracket those from the (n,γ) reaction, the present investigation giving the lower excitation energies. This systematic trend continues until at an excitation energy of about 3.5 MeV (the present limit) our results give values of E_x about 15 keV lower than those of Rapaport and Kerman; for lower excitation energies the difference is proportionately less. These small differences are well within the combined experimental uncertainties.

In general the present study is in good agreement with previously assigned l values, and we are able to make l-value assignments for several additional states in Ba^{139}. An apparent disagreement occurs for excitation energies around 1.29 MeV. A level at $E_x = 1.284$ MeV is clearly identified in the present investigation as being populated by an $l = 5$ transition. The γ line observed[40] at 1284 keV in the decay of Cs^{139} seems to be the ground-state transition from this level in Ba^{139}. Moragues *et al.*,[39] who investigated the $Ba^{138}(n,\gamma)Ba^{139}$ reaction, suggest a level at $E_x = 1292 \pm 1.5$ keV with a spin of $\frac{1}{2}$ or $\frac{3}{2}$. The suggested level appears consistent with the $l = 1$ transition reported by Wiedner *et al.*[4] at $E_x = 1.292$ MeV. However, our results give no indication of such a transition with the strength observed by Wiedner *et al.* at the same incident deuteron energy.

The spins of the $\frac{7}{2}^-$ ground state of Ba^{139} and of its $\frac{3}{2}^-$ level at $E_x = 0.630$ MeV, its $\frac{1}{2}^-$ level at $E_x = 1.084$ MeV, and its $\frac{5}{2}^-$ level at $E_x = 1.422$ MeV were inferred from the spins of the analog states in La^{139} – which have been determined by scattering experiments with polarized protons.[41] An additional level around $E_x = 1.70$ MeV, identified as $\frac{5}{2}^-$, is discovered in the present work to be a closely spaced doublet at $E_x = 1.682$ and 1.700 MeV, both with $l = 3$. The analog of this doublet was unresolved in the scattering experiment with polarized protons so that a $\frac{5}{2}^-$ assignment to either level is ambiguous. The $\frac{9}{2}^-$ assignments to $l = 5$ states in Ba^{139} were made from shell-model considerations. This assignment to the level at $E_x = 1.284$ MeV receives additional support from the $\frac{9}{2}^-$ assignment[42] to the level at $E_x = 1.40$ MeV in Nd^{143}; that these two levels correspond to each other can be seen from systematic shifts of the lower states in the $N = 83$ isotonic nuclei Xe^{137}, Ba^{139}, Ce^{141}, Nd^{143}, and Sm^{145} (Fig. 11).

The experimental cross sections for the $Ba^{138}(d,p)Ba^{139}$ reaction in Ref. 4 are ~30% larger than those measured in the present work. If these larger cross sections are used and a JULIE calculation identical to that in Ref. 4 is performed (without cutoff and with parameters identical to

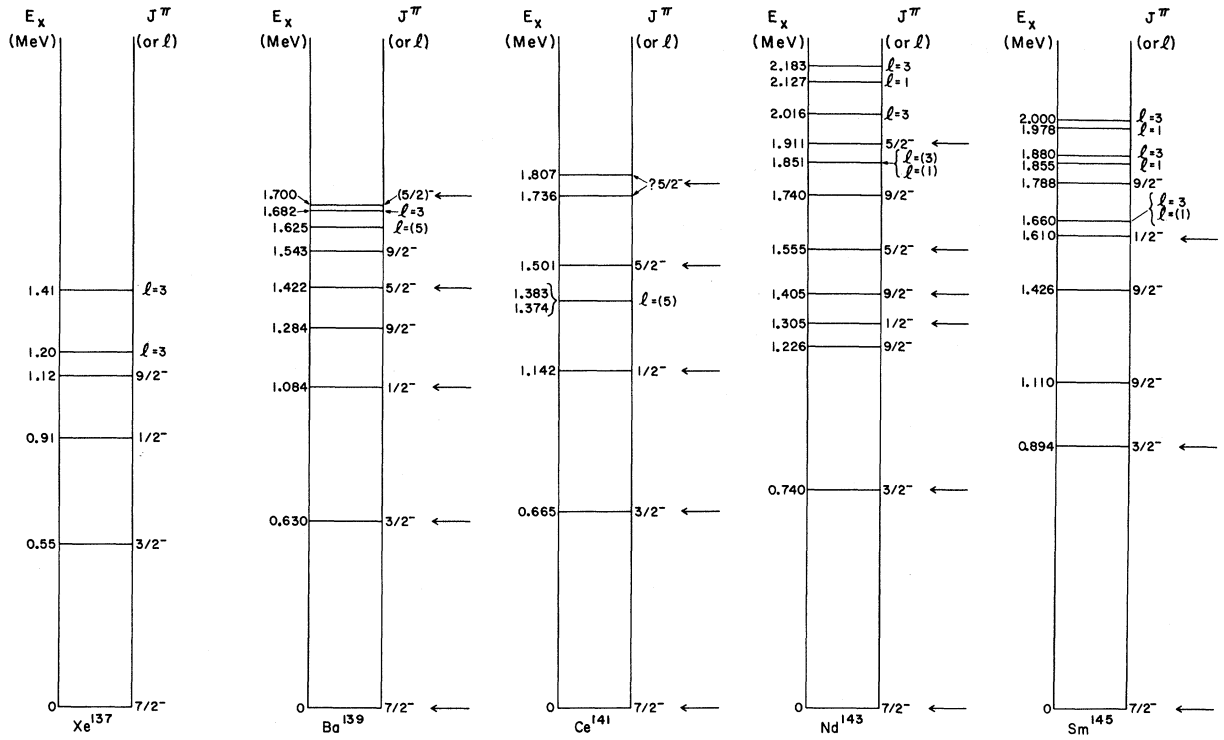

FIG. 11. Distribution of energy levels in $N=83$ isotonic nuclei, as compiled from Refs. 4, 6–8, 41, 42, 46 and the present work. Spin assignments based on polarization measurements are indicated by arrows. All firm $l=5$ transitions are given as $\frac{9}{2}^-$. In the Ce^{141} spectrum, the level to which the higher $\frac{5}{2}^-$ assignment belongs is uncertain, as discussed in Ref. 41.

those in Ref. 4), Eq. (1) leads to smaller values of S than are given in Ref. 4. In particular, for the transition to the $\frac{7}{2}^-$ ground state we obtain 0.64 instead of the reported 0.76; for the transition to the $\frac{3}{2}^-$ level at $E_x=0.63$ MeV we obtain 0.34 instead of the reported 0.49; and for the transition to the $\frac{1}{2}^-$ level at $E_x=1.08$ MeV we obtain 0.29 instead of the reported 0.41. We did not investigate how much of these discrepancies could be due to the fact that the spectroscopic factors in Ref. 4 were computed by substituting integrated cross sections in Eq. (1) instead of the maxima of the angular distributions.

The results obtained for the lighter isotopes are mostly new[43,44]; in the only previous (d,p) study,[1] the $Ba^{136}(d,p)$ reaction was examined in poor resolution. Our values of Q_0 (Table II) are more accurate than those in the Berkeley tabulation,[23] which were computed from mass tables for this region. In general the errors in the tabulated values are sufficiently large to encompass the present results; a surprising exception is the small error quoted for $Ba^{130}(d,p)$. Numerous new levels are observed and in many cases l-value assignments were possible. Most J assignments are made from the systematic shifts of the Q values of the levels in a comparison of the spectra of all isotopes (as in Fig. 10). The tentative $\frac{5}{2}^+$ assignments to the $l=2$ levels at $E_x=2.115$ MeV in Ba^{133} and at $E_x=2.524$ MeV in Ba^{131} are made from shell-model considerations. Those cases for which we compare with a level previously observed are noted in Tables IV–VII.

Our present limits in sensitivity (Sec. III) did not permit observation of any $l=4$ transitions corresponding to $\frac{7}{2}^+$ levels that have been tentatively identified in the energy region under investigation [e.g., at $E_x\approx1.4$ MeV in Ba^{137} (Ref. 1)]. This is not surprising because, as pointed out by Schneid, Prakash, and Cohen,[45] the $g_{7/2}$ orbit is already practically filled in the heavier Sn isotopes–i.e., in isotopes with neutron numbers greater than 72, which is less than the neutron number of our lightest Ba isotope ($N=74$ for the Ba^{130} target). Bruge *et al.*[44] observed only one $l=4$ state ($J^\pi=\frac{7}{2}^+$) at $E_x=2.236$ MeV in the $Ba^{138}(p,d)Ba^{137}$ pickup reaction.

As previously noted, the main purpose of this investigation is the comparison with our investigation of analog states.[9,12,14,16] For this reason, we concentrated on the relatively low-lying strong transitions and do not claim to give a complete listing of the weakly excited levels. For the same

reason, we did not try to exhaust the full single-particle strength of transitions to the various nuclear subshells in all investigated isotopes.

The observed distribution of strength, plotted against the Q values of the levels, is shown in Fig. 10 for each of the five target isotopes. The neutron shell closure at $N=82$ is clearly represented by the step in Q_0 between the Ba^{136} and the Ba^{138} targets and the disappearance of the low-lying $\frac{3}{2}^+$, $\frac{1}{2}^+$, and $\frac{11}{2}^-$ states (all seen in the isotopes with $N<82$) in the Ba^{139} spectrum. The spectroscopic factors S given in Fig. 10 were calculated with lower cutoff and with the bound-state well parameters $r_n = 1.20$ F and $a_n \approx 0.70$ F, as explained in Sec. IVA. For the levels without J assignments, S was obtained by dividing $(2J+1)S$ by 3 for $l=1$, by 5 for $l=2$, and by 7 for $l=3$ transitions. The arrow on each E_x scale indicates the limit of data evaluation.

Figure 11 shows the levels at low and medium excitation energies in the $N=83$ isotones Xe^{137}, Ba^{139}, Ce^{141}, Nd^{143}, and Sm^{145}. (The data are compiled from Refs. 4, 6–8, 41, 42, 46, and the present work.) The figure shows the excitation energy for each value of J^π and the small but systematic shift in this energy in going from one isotone to the next in this series. The $\frac{9}{2}^-$ level at $E_x = 1.284$ MeV in Ba^{139} fits the prediction of Ref. 46.

B. Comparison with Analog States

The comparison of the present results from the (d,p) reactions with the results on isobaric analog resonances in (p,p_0) scattering on the same target has two important features: (1) it yields Coulomb energy differences, and (2) it tests the equivalence of the spectroscopic factors S_{dp} and S_{pp_0} obtained from the two reactions. Both of these aspects are discussed in detail in a related paper[16] on elastic proton scattering, and the Coulomb energies are also given there. These topics will not be elaborated here. However, it can be noted that the dependence of S_{pp_0} on the rms radius, as found in the (p,p_0) analysis, is similar to that found here for S_{dp}; in particular, r_n and a_n are replaced by r_0 and a_0 – the radius and diffuseness parameters of the isospin-dependent nuclear well. Thus some of the largest uncertainty in the comparison of S_{dp} and S_{pp_0}, which stems from our ignorance of the geometrical parameters of the bound state, can be removed by comparing S_{dp} and S_{pp_0} at the same rms radius.

Figure 12 illustrates this comparison for the case of the $\frac{7}{2}^-$ ground state of Ba^{139} and its analog observed in the (d,p) and (p,p_0) reactions, respectively. The uncertainty (±20%) shown in the (d,p) reaction includes the facts that (1) the experimental error in the maximum of the angular distribution is about ±8%, (2) $S_{\text{cutoff}} \approx 1.25 S_{\text{FRNL}}$, and (3) S_{cutoff} computed with deuteron and proton parameters extrapolated from the results of Perey and Perey[31,32] is about 10% larger than the values of S computed with the parameters from Table VIII. The uncertainty (±20%) in S_{pp_0} represents the experimental error alone. The considerable overlap in S_{dp} and S_{pp_0} demonstrates the extent of agreement in the two methods of obtaining spectroscopic factors.

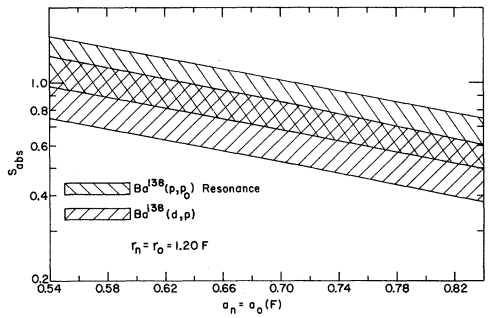

FIG. 12. Spectroscopic factors of the $\frac{7}{2}^-$ ground state of Ba^{139}, as obtained from the $Ba^{138}(d,p)$ reaction and from the analog-state resonance in the $Ba^{138}(p,p_0)$ reaction. The abscissa is the diffuseness $(a_n = a_0)$ of the respective potential wells. The uncertainties described in the text are indicated by the hatched areas.

C. Pairing Theory

As was shown in Sec. IVB, spectroscopic factors have substantial uncertainties. Nevertheless we intend to interpret one set of spectroscopic factors[47] within the framework of pairing theory[48,49] as a way of representing our results.

To use the formalism of pairing theory, we first compute the center-of-gravity energies (=quasiparticle energies) $E(J^\pi)$ for a particular spin and parity J^π by use of the relation

$$E(J^\pi) = \sum_i E_i(J^\pi) S_i(J^\pi) / \sum_i S_i(J^\pi) , \qquad (3)$$

where $E_i(J^\pi)$ is the excitation energy of an observed state i and $S_i(J^\pi)$ is its spectroscopic factor. Some values of $E(J^\pi)$ and $\sum_i S_i(J^\pi)$ computed from our data are plotted in Fig. 13, whose format is similar to that of Fig. 10. Most of the levels shown are ones whose single-particle strength can reasonably be assumed to be exhausted. Two exceptions are the $\frac{7}{2}^-$ level at $E_x = 1.794$ MeV and the $\frac{9}{2}^-$ level at $E_x = 3.141$ MeV in Ba^{137}; only a lower limit can be set on their values of $E(J^\pi)$. In interpreting the results in Fig. 13, it is useful to note that: (1) the $h_{9/2}$ level in Ba^{139} is computed without the questionable state at $E_x = 1.625$ MeV, (2) the well-known[43,44] $\frac{11}{2}^-$ level in Ba^{137} at $E_x = 0.66$ MeV is assumed to be

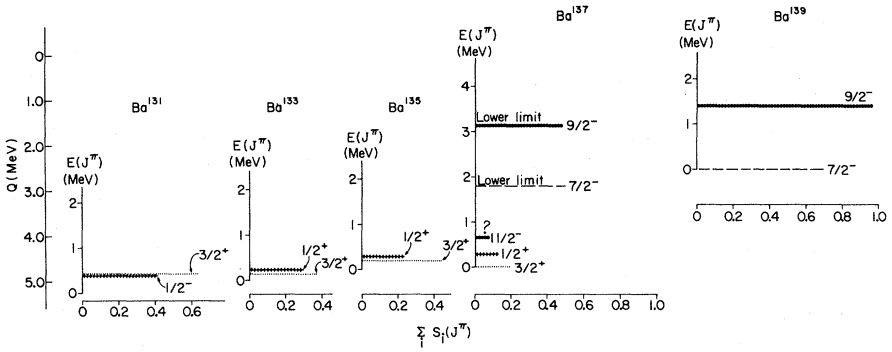

FIG. 13. The summed spectroscopic factors for single-particle configurations in the Ba isotopes, plotted at the energies of the centers of gravity computed from Eq. (3). The spectroscopic factors were calculated with cutoff and a bound-state neutron potential well of radius $r_n = 1.20$ F and diffuseness $a_n \approx 0.70$ F. The identification of l values is the same as that in Fig. 10.

the only strong level with this spin, (3) the uncertain and weak $\frac{1}{2}^+$ levels at $E_x = 1.839$ and 1.857 MeV in Ba^{137} were neglected, and (4) the $l = 2$ state at $E_x = 2.115$ MeV in Ba^{133} and at 2.524 MeV in Ba^{131} were omitted in computing $E(\frac{3}{2}^+)$ since their large separation from the other $l = 2$ states leads to the suspicion that they have $J^\pi = \frac{5}{2}^+$.

For states near the Fermi surface, values of $E(J^\pi)$ obtained from Eq. (3) are related to the difference $\epsilon(J^\pi) - \lambda$ between the single-particle energies $\epsilon(J^\pi)$ and the mean energy λ of the Fermi surface through the relation

$$E(J^\pi) - E(J_G^\pi) = \{[\epsilon(J^\pi) - \lambda]^2 + \Delta^2\}^{1/2} - \{[\epsilon(J_G^\pi) - \lambda]^2 + \Delta^2\}^{1/2}. \quad (4)$$

The energy 2Δ necessary to break a neutron pair is assumed to be 2.0 MeV and constant in the region from the Ba^{130} to Ba^{136} target isotopes.[50] $E(J_G^\pi)$ is the lowest center-of-gravity energy of spin and parity J_G^π (usually that of the ground state, as indicated by the subscript G); in this case $\epsilon(J_G^\pi)$ is the single-particle energy nearest to the Fermi surface. The "emptiness" $\sum_l S_l(J^\pi)$, i.e., the probability of finding a hole in the single-particle levels (in particular, around the Fermi surface) is predicted in pairing theory as

$$\sum_l S_l(J^\pi) = \tfrac{1}{2}\left(1 + \frac{\epsilon(J^\pi) - \lambda}{\{[\epsilon(J^\pi) - \lambda]^2 + \Delta^2\}^{1/2}}\right). \quad (5)$$

The predictions of this equation (with $\Delta = 1$ MeV) are shown (curved lines) in Fig. 14 for the target isotopes Ba^{130} to Ba^{136}. The relative positions of these curves are connected with the respective positions of the Fermi surface, since a single-particle level at the Fermi surface $[\epsilon(J^\pi) - \lambda = 0]$ is half filled $[\sum_l S_l(J^\pi) = 0.5]$ according to Eq. (5). For the target isotopes Ba^{130}, Ba^{134}, and Ba^{136}, the values $\epsilon(J_G^\pi) - \lambda$ were calculated from Eq. (5) by substituting the absolute spectroscopic factors $\sum_l S_l(J_G^\pi)$ in the left-hand side of this equation. The other $\epsilon(J^\pi) - \lambda$ for these target isotopes were subsequently computed from Eq. (4) by utilizing the centers of gravity from Eq. (3).

In the framework of the present approach, we assume constant relative positions of the single-particle levels in all isotopes under consideration. In view of the uncertainties in the spectroscopic factors and considering the possibility that levels may have been missed or a wrong J value may have been assumed, some deviations in the relative position of $\epsilon(J^\pi)$ in the different isotopes can be expected. From the data on Ba^{130}, Ba^{134}, and

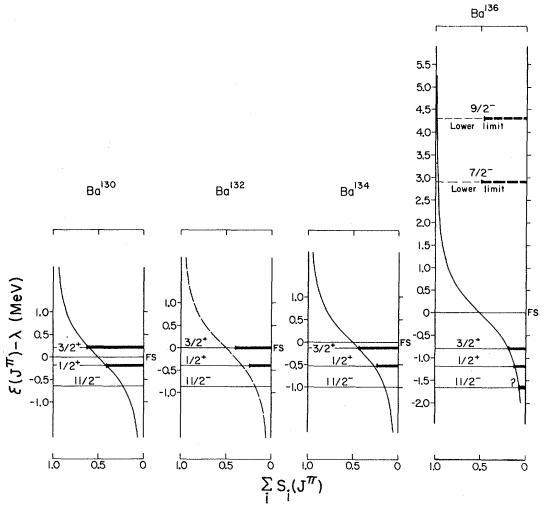

FIG. 14. Comparison of the summed spectroscopic factors (heavy horizontal bars) with the expectations from pairing theory (curves) for the Ba isotopes shown. The various single-particle levels $\epsilon(J^\pi)$ and the mean energies of the Fermi surface (FS) for each Ba isotope are indicated. The curves are calculated according to Eq. (5) with $\Delta = 1$ MeV.

Ba^{136} targets, an average value $\epsilon(\frac{3}{2}^+) - \epsilon(\frac{1}{2}^+) = 0.4 \pm 0.05$ MeV was obtained. The positions of these single-particle energies, $\epsilon(\frac{3}{2}^+)$ and $\epsilon(\frac{1}{2}^+)$ and also $\epsilon(\frac{11}{2}^-)$ obtained from Ba^{136} using Eq. (4), are plotted in Fig. 14. The sum of the observed absolute spectroscopic factors $\sum_l S_l(J^\pi)$ is represented by the length of a heavy bar. The differences between these lengths and the theoretical expectations given by the intersections of the single-particle energies $\epsilon(J^\pi)$ and the curves predicted by Eq. (5) test the consistency of the approach. The results for the $2d_{3/2}$ and $3s_{1/2}$ levels in the Ba^{130}, Ba^{134}, and Ba^{136} target isotopes appear very reasonable.

The data on the $Ba^{132}(d,p)Ba^{133}$ reaction are less reliable than those on the other isotopes, as has been noted previously. A comparison with the results from the neighboring isotopes leads to the approximate result $\lambda \approx \epsilon(\frac{3}{2}^+)$. The calculated distribution curve of this isotope is shown dashed in Fig. 14.

It is interesting to use Fig. 14 as an aid in evaluating the number of neutron holes present in the various single-particle levels. For example, in the Ba^{136} target, one would expect a total of two holes in and below the $d_{3/2}$ level (if the $f_{7/2}$ and higher levels are assumed to be empty). The number of holes, given by $\sum(2J+1)S$, adds up to 1.0 for the $d_{3/2}$ and $s_{1/2}$ levels. The remaining hole occurs in the $h_{11/2}$ level; the distribution curve intersects this level[51] at $\sum_l S_l(j) \approx 0.08$ which yields $(2J+1)S \approx 1$. A similar evaluation for Ba^{134} indicates that the distribution of the four holes expected is 1.7 in $d_{3/2}$, 0.5 in $s_{1/2}$, and 1.8 in $h_{11/2}$; for Ba^{130} the distribution of the eight holes expected is 2.5 in $d_{3/2}$, 0.9 in $s_{1/2}$, 2.8 in $h_{11/2}$, and 1.8 in other single-particle orbits.

The shell closure at $N = 82$ is responsible for a large gap in the energy spectrum of single-particle levels above the $d_{3/2}$ level, and hence the $f_{7/2}$ and $h_{9/2}$ levels are expected to lie high above the Fermi surface. Pairing theory is not applicable under these conditions. If we nevertheless use Eq. (4), we obtain lower limits on $\epsilon(\frac{7}{2}^-)$ and $\epsilon(\frac{9}{2}^-)$ (as shown in Fig. 14 for Ba^{136}) which are indeed high above the energy of the Fermi surface.

It should be noted that the preceding analysis assumes that $\Delta = 1$ MeV and, also, that the relative positions of the single-particle energies $\epsilon(J^\pi)$ remain the same for all isotopes considered. Both assumptions should be reasonable approximations for the range of isotopes considered here. Because of these approximations and the uncertainties in the spectroscopic factors, our comparison with the pairing theory is justified mainly by its usefulness in presenting a consistent description of part of our results.

VI. SUMMARY

The l values and excitation energies of many levels of the odd-mass Ba isotopes have been determined. Absolute spectroscopic factors for these levels were extracted by comparison of measured cross sections with DWBA calculations. With zero-range local potentials, the fits to the angular distributions were good when a sharp lower cutoff in the radial integrals was used – but were poor without the lower cutoff. Fits of intermediate quality were obtained with finite-range nonlocal potentials. The largest spectroscopic factors came from the cutoff calculations; the finite-range nonlocal calculations yielded ~15–20% lower values for the spectroscopic factors.

The spectroscopic factors are quite sensitive to the radius and diffuseness of the bound-state potential well. For $l \leq 3$, S is nearly constant if r_n and a_n are varied in such a way that the rms radius of the well remains constant. However, S decreases rapidly with increasing rms radius (~20% for a 3% increase in rms radius). For the $l = 5$ transitions, S is even more sensitive to r_n but less sensitive to a_n.

Since no wave functions have been calculated for the neutron states in this mass region, we have compared the systematics of our experimental results with a simple pairing model. The qualitative agreement with this model is good. However, many of the input parameters were rather arbitrary; more quantitative calculations are needed in this mass region.

The spectroscopic factors extracted in this paper will be compared in a subsequent paper with those extracted from measurements of analog-state resonances on the same targets. The degree to which some of the uncertainties can be eliminated by such a consistent analysis will be emphasized in that paper.

ACKNOWLEDGMENTS

We would like to thank C. E. Bolduc and the operating crew of the Argonne National Laboratory Tandem Van de Graaff for their cooperation in the performance of the experiment and J. A. Naser and L. A. Davis, Jr., for their help in the reduction of the data. In addition, we are grateful to Dr. J. P. Schiffer, Dr. D. Kurath, Dr. R. D. Lawson, and Dr. M. H. Macfarlane for many helpful discussions.

†Work performed under the auspices of the U. S. Atomic Energy Commission.

*Now also at the Physics Department, Northern Illinois University, DeKalb, Illinois 60115.

‡Present address: Department of Physics and Astronomy, University of Maryland, College Park, Maryland 20742.

§Present address: Physics Department, Rutgers – The State University, New Brunswick, New Jersey 08903.

[1]R. H. Fulmer, A. L. McCarthy, and B. L. Cohen, Phys. Rev. 128, 1302 (1962).

[2]F. W. Bingham and M. B. Sampson, Phys. Rev. 128, 1796 (1962); J. Rapaport and W. W. Buechner, Phys. Letters 18, 299 (1965).

[3]A. F. Jeans and W. J. Darcey, to be published.

[4]C. A. Wiedner, A. Heusler, J. Solf, and J. P. Wurm, Nucl. Phys. A103, 433 (1967).

[5]J. Rapaport and A. K. Kerman, Nucl. Phys. A119, 641 (1968).

[6]P. A. Moore, P. J. Riley, C. M. Jones, M. D. Mancusi, and J. L. Foster, Jr., Phys. Rev. 175, 1516 (1968).

[7]P. R. Christensen, B. Herskind, R. R. Borchers, and L. Westgaard, Nucl. Phys. A102, 481 (1967).

[8]R. K. Jolly and C. F. Moore, Phys. Rev. 145, 918 (1966).

[9]G. C. Morrison and Z. Vager, in Isobaric Spin in Nuclear Physics, edited by J. D. Fox and D. Robson (Academic Press Inc., New York, 1966), p. 320.

[10]G. C. Morrison, N. Williams, J. A. Nolen, Jr., and D. von Ehrenstein, Phys. Rev. Letters 19, 592 (1967).

[11]D. von Ehrenstein, G. C. Morrison, J. A. Nolen, Jr., and N. Williams, Bull. Am. Phys. Soc. 12, 714 (1967).

[12]N. Williams, G. C. Morrison, J. A. Nolen, Jr., and D. von Ehrenstein, Bull. Am. Phys. Soc. 12, 714 (1967).

[13]G. C. Morrison, N. Williams, J. A. Nolen, Jr., and D. von Ehrenstein, Bull. Am. Phys. Soc. 13, 70 (1968).

[14]N. Williams, D. von Ehrenstein, J. A. Nolen, Jr., and G. C. Morrison, in Proceedings of the Second Conference on Nuclear Isospin, Alisomar-Pacific Grove, 13-15 March 1969, edited by J. D. Anderson, S. D. Bloom, J. Cerny, and W. W. True (Academic Press Inc., New York, 1969), p. 695.

[15]P. von Brentano, N. Marquardt, J. P. Wurm, and S. A. A. Zaidi, Phys. Letters 17, 124 (1965).

[16]N. Williams, G. C. Morrison, J. A. Nolen, Jr., Z. Vager, and D. von Ehrenstein, to be published.

[17]J. F. Sharpey-Schafer, Phys. Letters 26B, 652 (1968).

[18]G. W. Greenlees, G. J. Pyle, and Y. C. Tang, Phys. Rev. 171, 1115 (1968).

[19]J. R. Erskine, Phys. Rev. 135, B110 (1964).

[20]J. T. Heinrich and T. H. Braid (unpublished).

[21]E. H. Auerbach, Brookhaven National Laboratory Report No. BNL-6562 (unpublished).

[22]J. R. Erskine, private communication.

[23]C. Maples, G. W. Goth, and J. Cerny, Nucl. Data A2, 429 (1966).

[24]G. R. Satchler, Nucl. Phys. 55, 1 (1964).

[25]L. L. Lee, Jr., J. P. Schiffer, B. Zeidman, G. R. Satchler, R. M. Drisko, and R. H. Bassel, Phys. Rev. 136, B971 (1964).

[26]R. H. Bassel, R. M. Drisko, and G. R. Satchler, Oak Ridge National Laboratory Report No. ORNL-3240, 1962 (unpublished); "Oak Ridge National Laboratory Memorandum to the Users of the Code JULIE," 1966 (unpublished).

[27]A maximum in the theoretical cross section is obtained with about 10% larger cutoff radius; the values at this maximum are about 2–8% larger than the values used here.

[28]R. M. Drisko, private communication.

[29]For $l=0$ distributions, the spectroscopic factors were obtained by comparing the cross sections at 5° instead of at the maxima of the angular distributions.

[30]The values of a_n actually used in the analyses for the different isotopes are given in the captions of Tables III–VII. They are grouped around $a_n = 0.70$ F and vary in such a manner that the rms radius $\langle R^2\rangle^{1/2}$ in Eq. (2) is proportional to $A^{1/3}$. Using $a_n = 0.70$ F instead of these values would change S by a maximum of about 2%.

[31]C. M. Perey and F. G. Perey, Phys. Rev. 132, 755 (1963).

[32]F. G. Perey, Phys. Rev. 131, 745 (1963).

[33]L. R. B. Elton, Nuclear Sizes (Oxford University Press, New York, 1961), Appendix C.

[34]W. C. Parkinson, D. L. Hendrie, H. H. Duhm, J. Mahoney, J. Saudinos, and G. R. Satchler, Phys. Rev. 178, 1976 (1969).

[35]J. C. Hiebert, E. Newman, and R. H. Bassel, Phys. Rev. 154, 898 (1967).

[36]G. E. Brown, J. H. Gunn, and P. Gould, Nucl. Phys. 46, 598 (1963).

[37]G. R. Satchler, private communication.

[38]Strictly speaking, the Gartenhaus potential (which yielded the normalization factor 1.65 used here) gives a range of about 1.5 F, but in the present cases the spectroscopic factors vary only ~1 – 2% over a variation of range from 1.25 to 1.58 F.

[39]J. A. Moragues, M. A. J. Mariscotti, W. Gelletly, and W. R. Kane, Phys. Rev. 180, 1105 (1969).

[40]T. Alväger, R. A. Naumann, R. F. Petry, G. Sidenius, and T. Darrah Thomas, Phys. Rev. 167, 1105 (1968).

[41]L. Veeser and W. Haeberli, Nucl. Phys. A115, 172 (1968).

[42]G. Clausnitzer, R. Fleischmann, G. Graw, D. Proetel, and J. P. Wurm, Nucl. Phys. A106, 99 (1968).

[43]Nuclear Data Sheets, compiled by K. Way *et al.* (Printing and Publishing Office, National Academy of Sciences – National Research Council, Washington, D. C.), No. NRC 59-2-23.

[44]G. Bruge, A. Chaumeaux, Ha Duc Long, and J. Picard, in Proceedings of the International Conference on Properties of Nuclear States, Montreal, Canada, 1969, edited by M. Harvey *et al.* (Presses de l'Université de Montréal, Montréal, Canada, 1969), p. 270.

[45]E. J. Schneid, A. Prakash, and B. L. Cohen, Phys. Rev. 156, 1316 (1967).

[46]S. Fiarman, E. J. Ludwig, L. S. Michelman, and A. B. Robbins, Nucl. Phys. A131, 267 (1969).

[47]The values of S_{cutoff} (column 6 of Tables III–VII) were chosen for this comparison, because the cutoff calculations yielded the best fits to the experimental angular distributions.

[48]L. S. Kisslinger and R. A. Sorenson, Kgl. Danske Videnskab. Selskab, Mat.-Fys. Medd. 32, No. 9 (1960).

[49]B. L. Cohen and R. E. Price, Phys. Rev. 121, 1441 (1961).

[50]The values of Δ can be calculated (Ref. 45) from the separation energies $E_S(n)$ of the last neutron by use of the relation

$$\Delta(n) = \tfrac{1}{4}[|E_S(n) - E_S(n-1)| + |E_S(n) - E_S(n+1)|],$$

where n is the number of neutrons in the nucleus for which Δ is calculated. With the values of Q_0 obtained in the present work (Table II), this formula yields $\Delta(81) = 0.98$ MeV for Ba^{137} and $\Delta(80) = 1.09$ MeV for Ba^{136}.

[51]The length of the heavy bar representing the observed $\sum_j S_l(J^\pi) \approx 0.08$ for the $h_{11/2}$ level in Ba^{137} is very questionable because we could not identify an $l=5$ angular distribution at the known position (Ref. 43) of this level. This uncertainty in the spectroscopic factor is indicated by question marks next to this level in Figs. 10, 13, and 14. The single-particle energies, $\epsilon(\frac{1}{2}^+) - \epsilon(\frac{11}{2}^-) \approx 0.47$ MeV, however, are not affected by this uncertainty in the spectroscopic factor because they are obtained from Eq. (4).

PHYSICAL REVIEW C VOLUME 1, NUMBER 6 JUNE 1970

Nuclear-Structure Studies with (d, t) Reactions on Pd^{110}, Pd^{108}, and Ru^{104}†

R. C. Diehl,* B. L. Cohen, R. A. Moyer, and L. H. Goldman‡
University of Pittsburgh, Pittsburgh, Pennsylvania 15213

(Received 2 January 1970)

Seventeen-MeV deuteron-induced (d,t) reactions on Pd^{110}, Pd^{108}, and Ru^{104} are used to complement (d,p) studies exciting the same final nuclei. Many new states are reported, and in several cases previous I-π assignments are changed. The sum of spectroscopic factors gives roughly the same degree of filling as was found from the (d,p) work for the s and d states; further anomalous behavior was found for the $g_{7/2}$ and $h_{11/2}$ states. There is a tendency for the spectroscopic strength to be shifted to higher excitation energy in (d,t) reactions than in (d,p) reactions. There are strong similarities between the Pd and Ru isotopes as regards the number of nuclear states of each I-π and the degree of filling of s and d states, but the $g_{7/2}$ state seems to be much less full in Ru than in Pd. In both Pd isotopes, there is a low-energy state (0.671 MeV in Pd^{109} and 0.781 MeV in Pd^{107}) excited by $l=1$ transitions in both (d,p) and (d,t) reactions, indicating that they probably include components with $2p$ holes *and* $3p$ particles.

INTRODUCTION

For many reasons, it is useful to complement spectroscopic studies with (d,p) reactions by analogous measurements with (d,t) reactions. This gives checks on l-transfer determinations, gives the j transfer when this is ambiguous, gives independent determinations of occupation numbers and single quasiparticle energies, etc.

A spectroscopic study of Pd^{107} and Pd^{109} by use of (d,p) reactions was reported from this laboratory[1] some time ago; the $Pd^{108,110}(d,t)$ reactions reported here were undertaken to complement that work. The $Ru^{104}(d,t)$ study was intended to complement experiments on the $Ru^{102}(d,p)$ reaction reported in preliminary form,[2] although the complete results of the latter are not yet available.

EXPERIMENTAL

Incident 17-MeV deuterons were obtained from the University of Pittsburgh three-stage Van de Graaff accelerator. The tritons were magnetically analyzed with an Enge split-pole spectrograph and detected with photographic emulsion plates in the focal plane of the spectrograph. Angular distributions were measured over an angular range from 10 to 35°. A detailed description of the scattering chamber and the spectrograph system is given in Ref. 1.

The impinging beam was collimated by a 1-mm-wide by 3-mm-high target slit. The antiscattering slit was 3 mm wide by 5 mm high. The Faraday-cup to slit current ratio averaged 30:1. The reaction products entered the spectrograph through an entrance aperture of 1.4 msr and were detected at the focal plane by 25-μ Kodak NTB plates.

The product of the incident beam times target thickness was measured by counting elastically scattered deuterons with NaI(Tl) scintillation detectors mounted at 38° on each side of the beam. This dual arrangement eliminates errors due to shifts in the angle of the incident beam. Elastic deuteron cross sections at these angles were determined with targets of sufficient thickness to make direct thickness measurements feasible, and they were checked by using these targets to measure elastic deuteron scattering at 11.8 MeV, where they are known from other work,[3] and at 7 MeV, where they can be assumed to be Rutherford